Calculations on vibrational predissociation of Ar–OH (A 2Σ+)

C. Chakravarty, D. C. Clary, A. Degli Esposti, and H.J. Werner

Citation: The Journal of Chemical Physics **95**, 8149 (1991); doi: 10.1063/1.461295
View online: http://dx.doi.org/10.1063/1.461295
View Table of Contents: http://scitation.aip.org/content/aip/journal/jcp/95/11?ver=pdfcov
Published by the AIP Publishing

Calculations on vibrational predissociation of Ar–OH ($A\,^2\Sigma^+$)

C. Chakravarty and D. C. Clary[a)]
University Chemical Laboratory, Lensfield Road, Cambridge CB2 1EW, England

A. Degli Esposti[b)] and H.-J. Werner
Fakultät für Chemie, Universität Bielefeld, 4800 Bielefeld, Germany

(Received 20 March 1991; accepted 26 June 1991)

An $\mathscr{R}$-matrix algorithm is developed for executing vibrational predissociation calculations within the Golden Rule approximation. The algorithm is used to calculate vibrational predissociation linewidths and OH product rotational distributions for the quasibound states of Ar–OH ($A\,^2\Sigma^+$, $v=1$). An *ab initio* potential energy surface obtained with the coupled electron pair approximation is used in the computations. The theoretical results are compared with experiment. The high anisotropy of the system is found to strongly favor vibrational to rotational energy transfer and the product OH ($A\,^2\Sigma^+$, $v=0$) molecules are produced in highly excited rotational states. Quasibound states associated with excited bending levels are predicted to dissociate more rapidly than those assigned to the ground bend. For metastable states with the same bending quantum number, linewidths are predicted to decrease with increase in the intermolecular stretching quantum number.

I. INTRODUCTION

A van der Waals dimer will posses one weak intermolecular bond, the breaking of which provides the most obvious dissociative route. Quantum states of the complex in which the intramolecular rovibrational energy of at least one of the monomers is greater than the van der Waals binding energy will be metastable with respect to dissociation of the van der Waals bond. The dissociation of a weakly bound complex in such a metastable state by a unimolecular process involving the transfer of excess intramolecular energy to the intermolecular stretching mode is known as vibrational predissociation. The study of the vibrational predissociation lifetimes and associated product distributions of van der Waals systems can provide useful information on intermolecular potential energy surfaces. Such dissociative processes also serve as a useful prototype for understanding unimolecular decay and intramolecular vibrational relaxation. The experimental and theoretical study of vibrational predissociation processes in weakly bound systems is, therefore, an active area of research.[1-9]

The spectra and dynamics of the Ar–OH complex has been the focus of much recent experimental and theoretical work. The complex is experimentally observable as well as sufficiently small for an accurate theoretical calculation of both the electronic potential energy surface and the rovibrational dynamics. In addition, it is an open-shell system and previous studies of van der Waals complexes with nonzero electronic angular momentum are not extensive.[10-14] We summarize previous theoretical and experimental work on the bound state spectra of the complex before discussing the reasons for interest in theoretical calculations on vibrational predissociation of Ar–OH ($A\,^2\Sigma^+$).

The Ar–OH complex was initially observed in matrix-isolation studies by Goodman and Brus.[15] The isolated-dimer in the gas phase was observed by laser-induced fluorescence spectroscopy in the region of the OH ($A^2\Sigma^+$) $\leftarrow$OH($X\,^2\Pi$) transition by Lester and co-workers[16-19] and also by Heaven and co-workers.[20] The dissociation energy, D_0, of the complex in the excited electronic state [asymptote:Ar($^1S_0$) + OH($A\,^2\Sigma^+$)] is about 750 cm^{-1} and an order of magnitude greater than the D_0 value for the ground electronic state [asymptote:Ar($^1S_0$) + OH($X\,^2\Pi$)]. An effective spectroscopic Hamiltonian for fitting the rotational band structure for complexes of open-shell diatomics was presented by Fawzy and Hougen[21] and an approximate potential energy surface was obtained by fitting the experimental electronic spectrum.[22] Observations by Bramble and Hamilton of the Ar–OH spectrum in a pulsed discharge system contain satellite bands displaced from the features of the main stretching progression by about 10 cm^{-1}, which could be due to hot bands from excited vibrational levels of the ground state.[23] Recently, Lester and co-workers have conducted stimulated emission pumping (SEP) experiments, which use a pump laser to selectively prepare van der Waals levels of the excited electronic state and a dump laser that induces transitions to vibrational levels of the ground electronics state.[24]

Ab initio potential energy surfaces for electronic states of the complex correlating with Ar($^1S_0$) + OH ($X\,^2\Pi$) and Ar($^1S_0$) + OH($A\,^2\Sigma^+$) were calculated using the coupled electron pair approximation (CEPA).[25,26] An accurate quantum-mechanical calculation for the rovibrational bound states and electronic spectrum of the complex using this potential has been carried out by us and the simulated spectrum agrees quite well with experiment.[27] The experimental and calculated D_0 values and vibrational frequencies for the excited electronic state differ by about 15%. These calculations indicated that some of the unassigned lines in the electronic spectrum close to dissociation were likely to be due to highly mixed bend–stretch combination bands. The effect of deuterium substitution and temperature on the rovi-

a) Author for correspondence.
b) Permanent address: Instituto di Spettroscopia Molecolare—C. N. R., Via de' Castagnoli, 1, 40126 Bologna, Italy.

brational band structure of the electronic transition was also studied theoretically.[28] The infrared spectrum of Ar–OH ($X\ ^2\Pi$), which has so far not been observed experimentally, has been predicted[29] and simulations of the SEP spectra have also been carried out.[24] Subsequent comparison with experiment indicated that the *ab initio* surface for the ground electronic state of Ar–OH reproduces the anisotropy of the potential fairly well but underestimates the well depth by at least 30%.[24] These theoretical calculations of the bound state spectra for ground and first excited electronic states have demonstrated that the *ab initio* potential is fairly accurate and have led to some new predictions.

The spectroscopic and *ab initio* studies have indicated that the first excited electronic state of Ar–OH is highly anisotropic and strongly bound for a van der Waals complex. Such an intermolecular potential would be expected to lead to significant coupling of the diatomic vibrational wave functions and result in a vibrational predissociation rate, which is large compared to the predicted decay rates for complexes such as the rare-gas hydrogen halides.[2-5] Since the *ab initio* potential has been demonstrated to be fairly accurate, it is of interest to study the effect of anisotropy and binding energy on vibrational predissociation lifetimes and product distributions by calculations of the rovibrational dynamics on this surface.

Vibrational predissociation in the excited electronic state was studied experimentally using dispersed fluorescence emission spectra and rotational linewidth measurements in the region of the OH A–X 1–0 transition.[30,31] The homogeneous contributions to the linewidths were derived to be of the order of 0.1 cm^{-1} corresponding to lifetimes of the order of 10 ps. The resolution of the dispersed fluorescence emission spectra was of the order of 60 cm^{-1} and consequently insufficient for obtaining unique product rotational distributions. The dependence of the Ar–OH interaction potential on the OH vibrational coordinate in the excited state was studied by comparing the vibrational spectra obtained by LIF in the OH A–X 0–0, 1–0, 1–1, and 2–1 regions and D_0 values were found to change by approximately 30 cm^{-1} on increasing the OH vibrational quantum number by unity. These experimental results are discussed in greater detail in Sec. V

Several theoretical approaches for treating vibrational predissociation have been developed. The predissociation of a metastable state prepared by optical excitation from an initial ground state may be viewed as a photodissociation process.[32] The calculation of the photodissociation cross sections over a range of frequencies without making any dynamical approximations is the most accurate way of studying predissociation lifetimes. The photodissociation spectrum will possess pronounced maxima at frequencies where metastable states or resonances are embedded in the continuum. Therefore, by considering the resonances generated by an inelastic scattering calculation one can obtain the positions, linewidths, and product state distributions associated with the decay of a metastable state without calculating the full photodissociation spectrum. Such a scattering or *S-matrix* approach is computationally more tractable than the calculation of the full photodissociation spectrum.[33] A further simplification commonly used in vibrational predissociation calculations is to treat the effect of the vibrational coupling due to the intermolecular interaction on the final scattering wave function to first order using perturbation theory.[1] This "Golden Rule" approach has been applied to $Ne–Cl_2$,[34] Ne–ICl,[35], He–ICl,[36] and $(HF)_2$,[37] and compares reasonably well with experiment considering the approximate nature of the potential energy surfaces. In the case of Ne–ICl, the results for the Golden Rule calculation agreed well with the results from a full photodissociation calculation. Previous studies have indicated that the Golden Rule approximation is reasonably good for van der Waals complexes with vibrational predissociation linewidths of about 0.01 cm^{-1}. Consequently, we have chosen to use the Golden Rule approach to model vibrational predissociation of Ar–OH ($A\ ^2\Sigma^+$). This method is also convenient because it is computationally relatively inexpensive and can be easily related to the previous bound state calculations.

The coordinate system and rovibrational Hamiltonian for a complex composed of an atom bound to an open-shell diatom is presented in Sec. II. The theory for vibrational predissociation within the Golden Rule approximation for an atom–diatom complex treated with the $\mathscr{R}$-matrix propagator method is described in Sec. III. The *ab initio* electronic structure calculations on the OH vibrational dependence of the Ar–OH ($A\ ^2\Sigma^+$) intermolecular potential are described in Sec. IV. In Sec. V we describe the results of our calculations for vibrational predissociation of Ar–OH($A\ ^2\Sigma^+$) and we compare them with the available experimental results. Conclusions are described in Sec. VI.

II. COORDINATES AND ROVIBRATIONAL HAMILTONIAN

The relative or internal coordinates of an atom–diatom complex can be measured with respect to a set of space-fixed (SF) axes.[38] The SF frame is defined to have the origin at the center of mass of the triatomic complex and the axes are oriented so as to be parallel with those in the laboratory reference frame. The Jacobi coordinates,[39] **r** and **R**, are most appropriate for describing the relative positions of the nuclei in a complex consisting of a diatom AB bound to an atom C. The coordinate **r** joins atom A to atom B, where A is the heavier nucleus of the diatom. The coordinate **R** joins the center of mass of the diatom AB to the atom C. The angle between the vectors **r** and **R** is designated θ. The spherical polar angles describing the orientation of **R** and **r** in the SF frame are $\hat{R} = (\theta'', \phi'')$ and $\hat{r} = (\theta', \phi')$, respectively. It should be noted that for Ar–OH, the $\theta = 0°$ orientation corresponds to the linear Ar–H–O geometry, whereas the $\theta = 180°$ orientation corresponds to the linear Ar–O–H geometry.

To construct the rovibrational Hamiltonian for a complex made up of a closed-shell atom and an open-shell diatom it is necessary to define an angular momentum coupling scheme. Since the perturbation due to the atom on the electronic states of the diatom is small for a weakly bound system, it is reasonable to regard the electronic angular momentum as being initially coupled to the rotational motion of the

diatom. The total diatomic angular momentum can then be coupled to the orbital angular momentum of the atom about the diatom to give the total angular momentum of the complex, which is a rigorously conserved quantity. The rovibrational states of the complex can then be correlated to the rovibrational states of the open-shell diatom. Using this angular momentum coupling scheme and separating out the motion of the center of mass of the system, the complete rovibrational Hamiltonian for an atom–diatom complex in a space-fixed (SF) reference frame can be written as

$$\hat{H} = -\frac{\hbar^2}{2\mu R}\frac{\partial^2}{\partial R^2}R - \frac{\hbar^2}{2\mu_{AB} r}\frac{\partial^2}{\partial r^2}r + \hat{H}_{rot}^{AB} + \frac{\hat{L}^2}{2\mu R^2} + V(R,r,\theta) + V_{AB}(r), \quad (1)$$

where μ_{AB} is the reduced mass of the diatom, μ is the reduced mass of the atom relative to the diatom, $\hat{H}_{rot}^{AB}$ is the sum of rotational and fine-structure Hamiltonians of the isolated diatom, $\hat{L}$ is the angular momentum vector associated with the rotation of **R**, $V(R,r,\theta)$ is the potential energy surface for the atom–diatom interaction, and $V_{AB}(r)$ is the electronic potential energy curve of the isolated diatom. The intermolecular potential for an atom interacting with a $^2\Sigma^+$ diatom can be expanded in terms of regular Legendre polynomials as[27]

$$V(R,r,\theta) = \sum_l V_\Sigma^l(R,r) P_l^0(\cos\theta). \quad (2)$$

III. THE GOLDEN RULE APPROXIMATION

A. First-order perturbation theory

The vibrational Hamiltonian, $\hat{H}_v$, of the isolated diatom has eigenfunctions $\{\phi_v(r)\}$, where v is the diatomic stretching vibrational quantum number such that[40]

$$\hat{H}_v\phi_v(r) = \left(-\frac{\hbar^2}{2\mu_{AB} r}\frac{\partial^2}{\partial r^2}r + V_{AB}(r)\right)\phi_v(r) = E_v^{AB}\phi_v(r). \quad (3)$$

The atom–diatom interaction potential $V(R,r,\theta)$ can couple the diatomic vibrational wave functions and allow for the transfer of energy from the intramolecular to the intermolecular stretching motion to give rise to vibrational predissociation.

When the vibrational predissociation process is slow, it is useful to define a model Hamiltonian such that the off-diagonal coupling of the diatomic vibrational wave functions by the intermolecular interaction potential is neglected.[1] The model Hamiltonian, $\hat{H}_0$, can be defined as

$$\hat{H}_0 = \sum_v |\phi_v\rangle\langle\phi_v|\hat{H}|\phi_v\rangle\langle\phi_v| = \sum_v |\phi_v\rangle\hat{H}_{vv}\langle\phi_v|, \quad (4)$$

where $\hat{H}$ is the complete rovibrational Hamiltonian of the atom–diatom complex defined in Eq. (1). The zeroth-order Hamiltonian, $\hat{H}_{vv}$, for particular vibrational state v is given by

$$\hat{H}_{vv} = -\frac{\hbar^2}{2\mu R}\frac{\partial^2}{\partial R^2}R + \frac{\hat{L}^2}{2\mu R^2} + \hat{H}_{rot,v}^{AB} + E_v^{AB} + V_{vv}(R,\theta). \quad (5)$$

Note that in our calculations we assume that the zero of the energy scale lies at the ground rovibrational energy of the isolated diatom. Further, we have not explicitly included the rotation–vibration coupling for the isolated diatom, but this is expected to be a minor correction. The vibrationally averaged interaction potential, $V_{vv}(R,\theta)$, decays to zero as R approaches infinity. The eigenfunctions of $\hat{H}_{vv}$ are denoted by $\psi_v(R,\hat{R},\hat{r})$ and can be regarded as zeroth-order approximation to the van der Waals vibrational wave functions associated with a given vibrational state of the diatom. The operator $\hat{H} - \hat{H}_0$, can be regarded as the perturbation term in the full Hamiltonian responsible for vibrational predissociation. Note that the vibrational matrix elements over the interaction potential can be expanded in terms of regular Legendre polynomials as

$$V_{vv'}(R,\theta) = \sum_l \langle v|V_\Sigma^l(R,r)|v'\rangle P_0^l(\cos\theta). \quad (6)$$

The complete wave function, $\Psi^{\mathscr{T}\mathscr{M}p}(\mathbf{R},\mathbf{r})$, is a solution of the time-independent Schrödinger equation,

$$[\hat{H}(\mathbf{R},\mathbf{r}) - E]\Psi^{\mathscr{T}\mathscr{M}p}(\mathbf{R},\mathbf{r}) = 0 \quad (7)$$

and may be expanded as a linear combination of the coupled-channel form,

$$\Psi^{\mathscr{T}\mathscr{M}p}(\mathbf{R},\mathbf{r}) = \sum_{v'}\phi_{v'}(r)\psi_{v'}(R,\hat{R},\hat{r}), \quad (8)$$

where $\mathscr{T}$ is the total angular momentum, $\mathscr{M}$ is the projection of the total angular momentum on a space-fixed axis, and p is the parity with respect to inversion through the origin of the SF coordinate system. Substituting from Eq. (8) in Eq. (7), multiplying by $\phi_v^*(r)$, and integrating over r, one obtains the following set of coupled differential equations,

$$(E - \hat{H}_{vv})\psi_v(R,\hat{R},\hat{r}) = \sum_{v'\neq v} V_{vv'}(R,\theta)\psi_{v'}(R,\hat{R},\hat{r}). \quad (9)$$

This set of coupled differential equations can be shown to be equivalent to the close-coupled equations for inelastic scattering.[41,42] The solution of the inelastic scattering equations to obtain scattering resonances and vibrational predissociation lifetimes has been well documented.[43–46] We are, however, interested in simplifying the problem further since, for weak predissociation, a solution of the final continuum wave functions accurate to first order in the coupling interaction is sufficient.

Consider a situation in which it is appropriate to model the vibrational predissociation process as a loss of one vibrational quantum on going from an initial vibrational state v_i to a final vibrational state v_f of the diatom. If one decouples the diatomic vibrational motion from the other rovibrational motions of the complex, one can write the initial, $\Psi_{v_i}^{\mathscr{T}\mathscr{M}p}$, and final, $\Psi_{v_f}^{\mathscr{T}\mathscr{M}p}$, wave functions for the system as[1,35]

$$\Psi_{v_i}^{\mathscr{T},\mathscr{M}p}(\mathbf{R},\mathbf{r}) = \phi_{v_i}(r)\psi_i(R,\hat{R},\hat{r}), \tag{10}$$

$$\Psi_{v_f}^{\mathscr{T},\mathscr{M}p}(\mathbf{R},\mathbf{r}) = \phi_{v_f}(r)\psi_f(R,\hat{R},\hat{r}). \tag{11}$$

This is known as the diabatic vibrational decoupling approximation. Using this approximation, one can omit the summation over v' in Eq. (9) and write

$$(E-\hat{H}_{v_iv_i})\psi_i(R,\hat{R},\hat{r}) = V_{v_iv_f}(R,\theta)\psi_f(R,\hat{R},\hat{r}), \tag{12}$$

$$(E-\hat{H}_{v_fv_f})\psi_f(R,\hat{R},\hat{r}) = V_{v_fv_i}(R,\theta)\psi_i(R,\hat{R},\hat{r}). \tag{13}$$

In order to obtain the solutions for the final state continuum wave functions accurate to first order in the coupling interaction (in this case $V_{v_fv_i}$), it is adequate to use the zeroth-order solution for the initial state $\psi_i(R,\hat{R},\hat{r})$.[47,48] This implies treating the initial metastable van der Waals rovibrational state $\psi_i(R,\hat{R},\hat{r})$ as a pure bound state by setting the right-hand side of Eq. (12) to zero. The bound state Schrödinger equation is then

$$\hat{H}_{v_iv_i}\psi_i(R,\hat{R},\hat{r}) = \epsilon_i\psi_i(R,\hat{R},\hat{r}). \tag{14}$$

In the case of weak coupling between the v_i and v_f manifolds, the bound state energy, ϵ_i, will be very close to the actual position of the resonant or metastable state. The set of discrete quasibound states determined using Eq. (14) can be considered to be weakly coupled to the continuum states defined by Eqs. (11) and (13). This combination of first-order perturbation theory and the diabatic vibrational approximation for vibrational predissociation has been termed the diabatic vibrational golden rule (DVGR) method.[1,35]

It is now necessary to determine the transition amplitude from a bound state i to a particular dissociative channel subject to the boundary condition that the final state continuum wavefunction must behave as a pure outgoing wave, and to relate the transition amplitude to the spectroscopic linewidth. Before proceeding with this, we summarize the basic assumptions underlying the DVGR approximation:[1] (i) interactions between discrete levels of different diatomic vibrational manifolds are negligible; (ii) continuum states belonging to different vibrational manifolds are assumed to be uncoupled; and (iii) the discrete-continuum coupling terms are assumed to be small compared with the spacings between the discrete levels; hence the use of first-order perturbation theory.

B. Quasibound states

The zeroth-order energies and wave functions for the quasibound states can be determined by solving the bound state equation defined in Eq. (14). Suitable radial and angular basis sets for diagonalizing the vibrationally averaged Hamiltonian, $\hat{H}_{v_iv_i}$ can be obtained by choosing suitable model stretching and angular potentials, $V_{\rm str}(R)$ and $V_{\rm ang}(\theta)$, respectively, such that one can write the full Hamiltonian as[49]

$$\hat{H} = \hat{H}_{\rm str} + \hat{H}_{\rm ang} + V_{v_iv_i}(R,\theta) - V_{\rm str}(R) - V_{\rm ang}(\theta). \tag{15}$$

The stretching or radial, $\hat{H}_{\rm str}$, and angular, $\hat{H}_{\rm ang}$, Hamiltonians can be diagonalized separately to provide optimal radial and angular basis sets. If $V_{\rm str}(R)$ and $V_{\rm ang}(\theta)$ are carefully chosen, then the effect of the bend–stretch or radial–angular coupling term, $V_{v_iv_i}(R,\theta) - V_{\rm str}(R) - V_{\rm ang}(\theta)$, can be minimized and the rovibrational Hamiltonian in Eq. (14) can be efficiently diagonalized using a relatively small direct product basis set of optimal radial and angular basis functions.

In order to generate an optimal radial basis, a stretching Hamiltonian $\hat{H}_{\rm str}$ is defined as

$$\hat{H}_{\rm str} = -\frac{\hbar^2}{2\mu R}\frac{\partial^2}{\partial R^2}R + V_{\rm str}(R), \tag{16}$$

where the choice of $V_{\rm str}(R)$ depends on the degree of anisotropy. For the strongly anisotropic Ar–OH($A\,^2\Sigma^+$) potential, we found that the best choice of $V_{\rm str}(R)$ was obtained by adiabatically separating the stretching and angular motion and equating $V_{\rm str}(R)$ to the effective radial potential corresponding to the angular wave function of lowest energy.[27] The eigenvalues of $\hat{H}_{\rm str}$ were determined using a basis set of equally distributed Gaussian functions.[50] The $N_{\rm str}$ radial eigenfunctions of lowest energy, $\{\psi_{\rm str}^k\}$, form the optimal radial basis.

The Hamiltonian, $\hat{H}_{\rm ang}$, used to determine the optimal angular basis set is obtained by taking the expectation value of terms of the full rovibrational Hamiltonian not included in $\hat{H}_{\rm str}$ over the lowest energy stretching wave function $\psi_{\rm str}^l$.[51] Therefore,

$$\hat{H}_{\rm ang} = \hat{H}_{\rm rot}^{\rm AB} + (\hat{L}^2/2\mu)\langle\psi_{\rm str}^l|1/R^2|\psi_{\rm str}^1\rangle + \langle\psi_{\rm str}^1|V_{v_iv_i}(R,\theta)|\psi_{\rm str}^1\rangle - \langle\psi_{\rm str}^1|V_{\rm str}(R)|\psi_{\rm str}^1\rangle. \tag{17}$$

It is necessary to consider the eigenfunctions of $\hat{H}_{\rm rot}^{\rm AB}$ and $\hat{L}^2$ in order to devise a suitable basis set to diagonalize $\hat{H}_{\rm ang}$. The rotoelectronic wave functions of the diatomic in a Hund's case (a) basis may be written as

$$|JM\bar{\Omega}\epsilon^{2S+1}\Lambda\rangle = (1/\sqrt{2})[|JM\Omega\rangle|\Lambda S\,\Sigma\rangle + \epsilon|JM-\Omega\rangle|-\Lambda S-\Sigma\rangle], \tag{18}$$

where J is the total angular momentum of the diatomic with projection M on a space-fixed axis and projection Ω on the diatomic internuclear axis $\mathbf{r}$.[52–55] Here S is the electronic spin angular momentum with projection Σ on $\mathbf{r}$. Also, Λ is the projection of the electronic orbital angular momentum on $\mathbf{r}$ and $\bar{\Omega} = |\Lambda+\Sigma|$. The symmetry index, $\epsilon = \pm 1$, is related to the parity of the rotoelectronic wave function with respect to inversion through the origin of the SF reference frame. For the $^2\Sigma^+$ state $\Lambda = 0$, $\Sigma = \frac{1}{2}$, and $\bar{\Omega} = \frac{1}{2}$. In conventional spectroscopic nomenclature the $\epsilon = +1$ and -1 states are designated F_1 and F_2, respectively,[56] and the diatomic rotoelectronic wave functions can be denoted by $|JMF_i\epsilon^2\Sigma^+\rangle$. The eigenfunctions of $\hat{L}^2$ are denoted by $|LM_L\rangle$, where L is the angular momentum quantum number associated with the rotation of $\mathbf{R}$ and M_L is the projection of $\mathbf{L}$ on a space-fixed axis. The complete angular basis set for the atom–diatom system can be written in terms of product wave functions of the form $|JMF_i\epsilon^{2S+1}\Lambda\rangle|LM_L\rangle$ of parity $\epsilon(-1)^{J+L-S}$. Since it is more convenient to consider an angular basis consisting of eigenfunctions of the parity operator $\hat{p}$, the total angular momentum $\mathscr{T}$, and its pro-

jection on a space-fixed axis $\mathscr{M}$, the angular basis used for optimization is[52]

$$|JLF_i\epsilon^{2S+1}\Lambda\mathscr{T}\mathscr{M}p\rangle = \sum_{MM_L}(JMLM_L|\mathscr{T}\mathscr{M})|JMF_i\epsilon^{2S+1}\Lambda\rangle|LM_L\rangle, \quad (19)$$

where $(\cdots|\cdots)$ denote the Clebsch–Gordan coefficients. The angular basis functions will also be denoted by

$$\Phi_a^{\mathscr{T}\mathscr{M}p}(\hat{R},r) = |JLF_i\epsilon^{2S+1}\Lambda\mathscr{T}\mathscr{M}p\rangle, \quad (20)$$

where a denotes collectively the angular momentum quantum numbers. The matrix elements over the potential with this basis are given in Ref. 27. For a given $\mathscr{T}$ and p, the $N_{\rm ang}$ angular wave functions of lowest energy, $\{\psi_{\rm ang}^{i\mathscr{T}\mathscr{M}p^{2S+1}\Lambda}\}$, constitute the optimal angular basis. The radial and angular basis sets can be optimized further to minimize bend–stretch coupling using an iterative procedure.[27]

The final bound-state wave function is expanded in the product radial-angular basis set as

$$\psi^{n\mathscr{T}\mathscr{M}p^{2S+1}\Lambda} = \sum_{k=1}^{N_{\rm str}}\sum_{i=1}^{N_{\rm ang}} d_{(i,k)}^{n\mathscr{T}p^{2S+1}\Lambda}\psi_{\rm ang}^{i\mathscr{T}\mathscr{M}p^{2S+1}\Lambda}\psi_{\rm str}^{k} \quad (21)$$

$$= \sum_{m=1}^{N_{\max}} d_m^{n\mathscr{T}p^{2S+1}\Lambda}\psi_{\rm ang}^{i\mathscr{T}\mathscr{M}p^{2S+1}\Lambda}\psi_{\rm str}^{k}, \quad (22)$$

where $m\equiv(i,k)$ identifies basis function m as the product of $\psi_{\rm str}^k$ and $\psi_{\rm ang}^{i\mathscr{T}\mathscr{M}p^{2S+1}\Lambda}$ and the total number of product basis functions, $N_{\max}$, is kept to a reasonable size by the requirement that $i+k\leqslant N_x$.

C. Coupled differential equations for the continuum states

The final state wave function, $\psi_f(R,\hat{R},\hat{r})$, can be expanded as

$$\psi_f(R,\hat{R},\hat{r}) = \sum_{a''}\Phi_{a''}^{\mathscr{T}\mathscr{M}p}(\hat{R},\hat{r})X_{a''v_f}^{a'v_f}(R), \quad (23)$$

where the angular basis functions, $\Phi_{a''}^{\mathscr{T}\mathscr{M}p}(\hat{R},\hat{r})$, were defined in Eq. (20). Note that the translational basis functions have been denoted by **X** in order to distinguish them from the radial channel functions, **G**, which are solutions of the set of coupled differential equations for inelastic scattering (see Sec. III D). In the remainder of this paper the subscript labeling the vibrational quantum number, v, of the diatomic has been dropped since we consider continuum states associated with a single value v_f of v. Substituting the expression for $\psi_f(R,\hat{R},\hat{r})$ from Eq. (23) in Eq. (13), multiplying by $[\Phi_a^{\mathscr{T}\mathscr{M}p}(\hat{R},\hat{r})]^*$ and integrating over $\hat{R}$ and $\hat{r}$ leads to the following set of coupled differential equations in matrix form:

$$\left[\frac{\partial^2}{\partial R^2} + \mathbf{k}^2 - \frac{L(L+1)}{R^2}\mathbf{I} - \mathbf{U}(R)\right]\mathbf{X}(R) = \frac{2\mu}{\hbar^2}\lambda(R), \quad (24)$$

where

$$[\mathbf{k}]_{aa''}^2 = \delta_{aa''}\frac{2\mu}{\hbar^2}(E - E_{v_f}^{\rm AB} - E_{v_fJF_i\epsilon}^{\rm AB}), \quad (25)$$

$$[\mathbf{U}(R)]_{aa''} = \frac{2\mu}{\hbar^2}\int[\Phi_a^{\mathscr{T}\mathscr{M}p}(\hat{R},\hat{r})]^* V_{v_fv_f}(R,\theta) \times\Phi_{a''}^{\mathscr{T}\mathscr{M}p}(\hat{R},\hat{r})d\hat{R}\,d\hat{r}, \quad (26)$$

$$[\lambda(R)]_{ai} = \int[\Phi_a^{\mathscr{T}\mathscr{M}p}(\hat{R},\hat{r})]^* V_{v_fv_i}(R,\theta)\psi_i(R,\hat{R},\hat{r})d\hat{R}\,d\hat{r}, \quad (27)$$

L is the orbital angular momentum quantum number associated with channel a, and **I** is the unit matrix. Note that the presence of the driving term, λ, implies that Eq. (24) corresponds to a set of inhomogeneous coupled differential equation.

The form of Eq. (24) is analogous to the coupled differential equations obtained by Heather and Light for direct photodissociation of a triatomic.[57] In their case the transition takes place between two electronic states and expansion of the final state wave function includes fragment vibrational as well as rotational wave functions. The driving term in our calculations stems from the off-diagonal vibrationally averaged matrix elements over the interaction potential. Since this is a predissociation process from a well-defined, initially prepared metastable state, this coupling term is a zero-rank tensor[47] and the selection rules for vibrational predissociation are

$$\Delta\mathscr{T} = 0, \qquad p\leftrightarrow p', \quad p = p'. \quad (28)$$

The calculation of the matrix elements defined in Eqs. (25)–(27) proves particularly straightforward for atom–diatom complexes since both the bound and continuum wave functions can be efficiently computed using Jacobi coordinates. The diagonal and off-diagonal vibrationally averaged matrix elements over the potential, $V_{v_fv_f}(R,\theta)$ and $V_{v_fv_i}(R,\theta)$, respectively, can be expanded in terms of reduced rotation matrices or Legendre polynomials. The driving term, $\lambda(R)$, is a column vector for a given initial bound state wave function, $\psi_i(R,\hat{R},\hat{r})$, with elements labeled by the fragment rotational quantum state. Expanding $\psi_i(R,\hat{R},\hat{r})$ as

$$\psi_i(R,\hat{R},\hat{r}) = \sum_{m=1}^{N_{\max}} d_m^{n\mathscr{T}p^{2S+1}\Lambda}\psi_{\rm ang}^{i\mathscr{T}\mathscr{M}p^{2S+1}\Lambda}(\hat{R},\hat{r})\psi_{\rm str}^k(R) = \sum_{m}^{N_{\max}} d_m^{n\mathscr{T}p^{2S+1}\Lambda}\psi_{\rm str}^k(R)\sum_{a'}c_{a'}^i\Phi_{a'}^{\mathscr{T}\mathscr{M}p}(\hat{R},\hat{r}), \quad (29)$$

where $m\equiv(i,k)$ identifies basis function m as the product of $\psi_{\rm str}^k$ and $\psi_{\rm ang}^{i\mathscr{T}\mathscr{M}p^{2S+1}\Lambda}$. Expanding $V_{v_fv_i}(R,\theta)$ in terms of reduced rotation matrices, allows one to rewrite Eq. (27) as

$$[\lambda(R)]_a = \sum_{m}^{N_{\max}} d_m^{n\mathscr{T}p^{2S+1}\Lambda}\psi_{\rm str}^k(R)\sum_{l,m}V_{v_fv_i}^{l,m}(R)\sum_{a'}c_{a'}^i \times\int[\Phi_a^{\mathscr{T}\mathscr{M}p}(\hat{R},\hat{r})]^* P_0^l(\cos\theta) \times\Phi_{a'}^{\mathscr{T}\mathscr{M}p}(\hat{R},\hat{r})d\hat{R}\,d\hat{r}. \quad (30)$$

The integral on the right-hand side can once again be obtained using Eq. (21).

D. Transition amplitudes, lifetimes, and linewidths

As discussed in the previous section, the set of coupled differential equations [Eq. (24)] for vibrational predissociation is analogous to the coupled differential equations obtained by Heather and Light for direct photodissociation involving two electronic states.[57] It can be shown by using a similar derivation to that of Ref. 57 that the transition amplitude from an initial bound state to a dissociative channel can be related to the overlap of the driving term with scattering wave functions associated with the final vibrational manifold and hence can be used to calculate vibrational predissociation linewidths.[58]

Therefore, if

$$(\mathbf{C}' + i\mathbf{S}')$$

is the transition amplitude matrix, it can be shown that

$$(\mathbf{C}' + i\mathbf{S}') = -\mu^{-1/2}\mathbf{k}^{-1/2}(\mathbf{C}^T - i\mathbf{S}^T)^{-1} \times \int_0^\infty dR\, \mathbf{G}^T(R)\lambda(R). \tag{31}$$

When calculating spectroscopic vibrational predissociation linewidths, it is assumed that optical excitation from some initial ground state will favor the transition to the metastable or quasibound state rather than to the continuum.[1] The optical transition to the metastable state will then result in a Lorentzian line shape given by[1]

$$I(E) = \frac{[\Gamma_i(E)/2]}{[E - E_i(E)]^2 + [\Gamma_i(E)/2]^2}, \tag{32}$$

where $I(E)$ is the intensity as a function of energy, E, of the exciting radiation, Γ_i is the linewidth of the resonance, and $E_i(E)$ is the position of the resonance. The linewidth, Γ_i, is more precisely defined as the full width of the resonance at half-maximum (FWHM). If the resonances can be assumed to be isolated narrow resonances such that the linewidth of the predissociating state is much smaller than the separation between adjacent resonances, then $\Gamma_i(E)$ and $E_i(E)$ can be assumed to be constant parameters characterizing resonance i. Further, if the discrete-continuum couplings are sufficiently weak to justify first-order perturbation theory then E_i can be written as the sum of ϵ_i, the energy of the metastable state derived from the bound-state calculation, and Δ_i, the level shift due to the introduction of discrete-continuum coupling. The lifetime of the state is given by $\hbar/\Gamma_i$. The linewidth, Γ_i, of the resonance is the sum of the partial linewidths Γ_{ij} due to dissociation into an open channel j. If the regular scattering solution associated with a particular open channel j is defined to be

$$\chi_j(R,\hat{R},\hat{r}) = \sum_{\alpha'} \Phi_{\alpha'}^{\mathcal{J},M_P}(\hat{R},\hat{r}) G_{\alpha'}^j(R), \tag{33}$$

then it can be shown using the Feshbach resonance theory[33,59] for a single discrete level coupled to a set of continua that

$$\Gamma_{ij} = 2\pi \left| \int \psi_i(R,\hat{R},\hat{r}) V_{v_i p_i}(R,\theta) \chi_j(R,\hat{R},\hat{r}) d\tau \right|^2, \tag{34}$$

where the scattering solutions are normalized to a δ function of energy and calculated at a single energy corresponding to the quasibound state energy ϵ_i. The overlap integral in Eq. (34) corresponds to exactly the same integral as in Eq. (31), except that in the derivation of Eq. (31) the continuum wave functions were assumed to be normalized to $\pi/2$ times a δ function of energy. Therefore, using Eqs. (31) and (34), the partial linewidth for dissociation from an initial state i to an open channel j can be written as

$$\Gamma_{ij} = 4|[(\mathbf{C}' + i\mathbf{S}')]_{ij}|^2. \tag{35}$$

The total linewidth for resonance i is given by

$$\Gamma_i = \sum_j \Gamma_{ij}, \tag{36}$$

and the probability for dissociation into channel j is

$$P_j = \Gamma_{ij}/\Gamma_i. \tag{37}$$

The $\mathscr{R}$- matrix methods used for photodissociation[57,60–68] can be adapted with only minor modifications to solve VP problems within the Golden Rule approximation. The crucial advantage of such a technique is that it allows the scattering wave function and the overlap integral between the scattering and bound wave functions to be propagated simultaneously (a single-pass calculation). The details of the R-matrix algorithm for vibrational predissociation can be found in Ref. 58 (also see Refs. 57 and 67).

IV. *AB INITIO* POTENTIAL FOR Ar–OH ($A\,^2\Sigma^+$)

The *ab initio* calculations to determine the OH vibrational dependence of the Ar–OH ($A\,^2\Sigma^+$) intermolecular potential were carried out using the coupled electron pair approximation (CEPA)[25] with a very large basis set. The details of the basis set composition can be found in Ref. 26. *Ab initio* points were calculated at $r = 1.85$, 1.95, and 2.05 bohr. For each value of r, electronic energies were obtained for R values distributed over a range of 3.0–13.0 bohr and for $\theta = 0°$, 45°, 90°, 135°, and 180°. The *ab initio* energies for $r = 1.85$ and $r = 2.05$ bohr are given in Tables I and II, respectively. The *ab initio* energies for $r = 1.95$ bohr are given in Ref. 26. The *ab initio* points were fitted to the form[55]

$$V(R,r,\theta) = \sum_{n=1}^{N} \sum_{l=1}^{L} d_{m0}^{l+m-1}(\theta) A_{ln}(R)(r - r_e)^{n-1} = \mathbf{p}^T \cdot \mathbf{A}(R) \cdot \mathbf{s}, \tag{38}$$

where N is the number of values of the OH bond distance and L is the number of values of θ at which the *ab initio* potential was calculated. For a complex consisting of a structureless atom bound to a diatom in a $^2\Sigma$ electronic state, m is set to zero. The vectors $\mathbf{p}$ and $\mathbf{s}$ have the elements

$$p_l = d_{m0}^{l+m-1}(\cos\theta), \quad s_n = (r - r_e)^{n-1}. \tag{39}$$

The matrix $\mathbf{A}$ can be expressed as

$$\mathbf{A}(R) = \mathbf{P}^{-1} \cdot \mathbf{B}(R) \cdot \mathbf{S}^{-1}, \tag{40}$$

where $P_{lk} = d_{m0}^{l+m-1}(\cos\theta_k)$, $S_{nm} = (r_m - r_e)^{n-1}$, and θ_k and r_m are the angles and bond distances at which the potential has been calculated. At each value of θ_k and r_m, the R-dependent terms were fitted independently to functions of the form

TABLE I. CEPA(1) interaction potential V_Σ (in cm^{-1}) of OH + Ar for an OH bond distance $r = 1.85$ bohr as function of R (in Å) and θ (in degrees).[a]

R	θ 0	45	90	135	180
1.59	442 600.63	90 371.16	76 666.00	61 701.22	33 655.91
1.70					10 113.50
1.90					1 192.22
2.00		17 047.73	19 259.91	10 181.69	− 515.66
2.10	16 997.70				− 1 240.64
2.20		7 593.34	9 857.06	4 250.20	− 1 377.61
2.30	4 763.42				− 1 228.46
2.50	522.51	2 068.66	3 391.80	1 255.87	− 771.46
2.60	− 302.51				
2.70	− 700.16	755.70	1 569.79	517.85	
2.80	− 850.26				
2.90	− 864.43	185.42	673.35	162.20	
3.00	− 809.97				− 262.58
3.10		− 44.24	247.43	1.91	
3.20	− 633.57	− 94.51	131.60	− 37.43	
3.30		− 120.56	55.35	− 60.19	
3.50	− 389.79	− 131.82	− 23.57	− 75.84	− 122.04
4.00	− 161.55	− 96.80	− 51.08	− 55.21	− 57.81
5.00	− 32.78	− 22.41	− 17.56	− 16.26	− 14.69
6.00	− 9.15	− 6.79	− 5.54	− 5.19	− 4.76

[a] R is the distance from the Ar atom to the center of mass of OH. θ is the angle between the **r** and **R** vectors. $\theta = 0°$ and $\theta = 180°$ correspond to the linear OH–Ar and Ar–OH structures, respectively.

$$B_{ln}(R) = \exp[-a_l(R-R_l)]\cdot\left[\sum_{i=0}^{3} b_l^{(i)} R^i\right] - \tfrac{1}{2}\{1+\tanh[(R-S_l)/T_l]\}\cdot\left[\sum_{i=3}^{4} c_l^{(2i)} R^{-2i}\right]. \quad (41)$$

The parameters a_l and R_l were determined, assuming an exponential short-range repulsion term, from the energies at the two smallest OH–Ar distances. The parameters S_l and T_l are switching functions that damp the long-range part at small R. The parameters b_l and c_l are obtained for fixed R_l, S_l, and T_l by a least-square fitting procedure. The coefficients of the fit can be obtained from the authors on request. The vibrationally averaged matrix elements were obtained by integration over r,

$$V_{vv'}(R,\theta) = \langle v(r)|V(R,r,\theta)|v'(r)\rangle, \quad (42)$$

TABLE II. CEPA(1) interaction potential V_Σ (in cm^{-1}) of OH + Ar for an OH bond distance $r = 2.05$ bohr as function of R (in Å) and θ (in degrees).[a]

R	θ 0	45	90	135	180
1.59	761 242.21	92 887.68	77 150.01	60 865.80	27 310.21
1.70					11 507.29
1.90					2 474.53
2.00		16 449.69	19 545.35	11 222.37	605.07
2.10	23 510.05				− 296.66
2.20		7 105.92	10 044.07	4 943.54	− 622.07
2.30	6 051.25				− 659.42
2.50	304.45	1 779.66	3 438.61	1 493.51	− 500.82
2.60	− 752.37				
2.70	− 1 226.96	574.40	1 586.66	611.24	
2.80	− 1 370.02				
2.90	− 1 335.57	74.64	678.23	191.98	
3.00	− 1 216.31				− 246.65
3.10		− 113.27	247.99	9.37	
3.20	− 912.42	− 149.81	130.87	− 34.06	
3.30		− 165.22	53.64	− 59.22	
3.50	− 537.66	− 161.28	− 26.45	− 77.43	− 125.17
4.00	− 214.13	− 98.03	− 54.01	− 57.83	− 60.71
5.00	− 41.74	− 25.97	− 18.64	− 17.29	− 15.69
6.00	− 11.39	− 7.81	− 5.88	− 5.55	− 5.12

[a] R is the distance from the Ar atom to the center of mass of OH. θ is the angle between the **r** and **R** vectors. $\theta = 0°$ and $\theta = 180°$ correspond to the linear OH–Ar and Ar–OH structures, respectively.

where the OH vibrational functions were obtained by Numerov integration[71] from the RKR potential.[72] The relevant $\langle v|(r-r_e)^n|v'\rangle$ matrix elements are given in Table III.

V. VIBRATIONAL PREDISSOCIATION OF Ar–OH ($A\ ^2\Sigma^+$)

Vibrational predissociation lifetimes for Ar–OH ($A\ ^2\Sigma^+$) have been experimentally determined by the study of spectroscopic linewidths in the LIF spectra. In Sec. V A we summarize the main experimental results. In Sec. V B we provide the computational details relevant for our calculations on vibrational predissociation in Ar–OH ($A\ ^2\Sigma^+$) using the Golden Rule approximation. We also describe some calculations we have performed on the Ne–ICl system to check our computer program for calculating vibrational predissociation linewidths. In Sec. V C our calculated results are discussed and compared with experiment. A set of approximate calculations that investigate the effect of anisotropy of the intermolecular potential on the vibrational predissociation lifetimes is presented in Sec. V D. In Sec. V E we consider the effect of deuterium substitution on the vibrational predissociation linewidths of the complex.

A. Experimental results

The homogeneous contributions to the linewidths, Γ, and the corresponding lifetimes determined experimentally from the main stretching progression features in the OH A–X 1–0 region[30,31] by Berry *et al.* are shown in Table IV. The linewidths for levels with $v_s = 0$ to 4 are of the order of 0.1 cm^{-1}. The linewidths for levels with $v_s = 5$ and 6 decrease sharply by at least an order of magnitude. The experimental uncertainty of the linewidths is fairly large and prevents establishment of any clear trends in linewidths for $v_s \leqslant 3$. The spectroscopic line positions indicate that the D_0 values increases by 32 cm^{-1} and decreases by 22 cm^{-1} for OH in the first and second excited vibration state with respect to the ground vibrational state. Fawzy and co-workers have also obtained spectroscopic linewidth measurements, but they have not extracted the homogeneous contribution.[73] The average spectral linewidth obtained by them for rotational levels associated with the main stretching progression features of Ar–OH ($A\ ^2\Sigma^+$, $v=0$) and Ar–OH ($A\ ^2\Sigma^+$, $v=1$) are 0.10 cm^{-1} and 0.17 cm^{-1}, respectively. The corresponding values for Ar–OD ($A\ ^2\Sigma^+$, $v=0$) and Ar–OD ($A\ ^2\Sigma^+$, $v=1$) are 0.10 and 0.11 cm^{-1}, respectively. The main significance of their results is the indication that substitution of OH by OD decreases the predissociation linewidths. We also note that a study of fluorescence decay lifetimes in Ar–OH ($A\ ^2\Sigma^+$) indicates the possibility of electronic predissociation in the OH but not in the OD complex[74] for the vibrational ground state; implications of this for extracting the homogeneous contribution due to vibrational predissociation from observed linewidths is not yet clear.

TABLE III. Vibrational matrix elements for OH ($A\ ^2\Sigma^+$) (in a.u., r_e = 1.95 bohr).

v	v'	$\langle v\|(r-r_e)\|v'\rangle$	$\langle v\|(r-r_e)^2\|v'\rangle$
0	0	0.004 749	0.020 910 8
0	1	0.143 230	0.009 169 0
1	1	0.087 350	0.071 628 2

TABLE IV. Experimentally determined homogeneous contributions to the linewidth (Γ) and vibrational predissociation lifetimes (τ) of the main progression features in the OH 1–0 region.[31] The intermolecular stretching quantum number, v_s, from the experimental assignment is shown.

v_s	Γ (cm^{-1})	τ (ps)
0	0.140–0.233	23–38
1	0.210–0.255	21–25
2	0.140–0.297	18–38
3	0.199–0.308	17–27
4	0.090–0.189	28–59
5	$\leqslant$0.064	$\geqslant$83
6	$\leqslant$0.034	$\geqslant$156

Due to low resolution of the dispersed fluorescence spectra of the OH ($A\ ^2\Sigma^+$, $v=0$) produced on excitation of van der Waals levels of Ar–OH ($A\ ^2\Sigma^+$, $v=1$), Lester and co-workers did not obtain unique vibrational predissociation product distributions.[31] Their dispersed fluorescence spectra can be sufficiently resolved, however, to indicate an abrupt cutoff in the population of OH levels at $N=7$ when the main progression features with $v_s = 3$–6 were excited. Excitation of a nonprogression feature expected to involve excited bending states of the complex (labeled feature A in Ref. 31) appeared to result in significant population of levels with $N=8$ and 9 and a minimum in the population distribution at low N. (Note that experimental rotational distributions are given as a function of the integral rotational angular momentum quantum number N of the $^2\Sigma$ diatom rather than the half-integral total diatomic angular momentum quantum number J.)

B. Details of calculation and convergence tests

Experimental studies of the fragmentation of Ne–ICl in the region of the ICl ($B\ ^3\Pi_{0+}$, $v=2$) excited state have been conducted by Lester and co-workers.[69] A quasibound vibrational state of Ne–ICl ($B\ ^3\Pi_{0+}$, $v=2$) is produced by optical excitation and fragments by a vibrational predissociation process to yield primarily ICl ($B\ ^3\Pi_{0+}$, $v=1$). Roncero *et al.* have carried out an exact three-dimensional (3D) quantum mechanical study to obtain the photofragmentation for Ne–ICl, which agree well with the experiment.[35] They have also compared the 3D results with the results obtained by combining the vibrational diabatic decoupling and Golden Rule approximations (abbreviated as DVGR) and found good agreement. The DVGR results were obtained by separately calculating the bound and continuum solutions associated with the $v=2$ and $v=1$ vibrational manifolds, respectively, and then computing the overlap integral to evaluate Γ_{ij} as defined in Eq. (34). Since our $\mathscr{R}$-matrix code was designed to implement the DVGR method, we decided to test the code against the results obtained previously for

Ne–ICl. The ICl vibrational wave functions and stretching basis set were both generated using distributed Gaussian basis sets (for more details see Ref. 58).

The angular Hamiltonian as defined in Eq. (15), was diagonalized using 41 basis functions. The matrix elements over the interaction potential can be found in Ref. 70. In order to obtain the final rovibrational energies and wave functions, a basis set with $N_{\rm str} = 15$, $N_{\rm ang} = 30$, and $N_x = 45$ was used. Approximate intermolecular stretching, v_s, and bending, v_b, quantum numbers could be assigned for the lowest vibrational levels of the complex. Our values for the binding energies of the $v_s = 0$, $v_b = 0$, and $v_s = 0$, $v_b = 1$ levels were $-42.3631\ \text{cm}^{-1}$ and $-34.7985\ \text{cm}^{-1}$, respectively, which agree well with the values of $-42.3613\ \text{cm}^{-1}$ and $-34.8464\ \text{cm}^{-1}$ given in Ref. 35.

The $\mathscr{R}$-matrix calculations for lifetimes and product rotational distributions were carried out for zero total angular momentum and positive parity. The total number of rotational channels associated with the continuum states was set to 41. With the initial and final values of the scattering coordinate, R, fixed at 5.5 and 24.0 bohr, respectively, and a constant sector width of 0.03 bohr, the halfwidths obtained for the $v_s = 0$, $v_b = 0$ and $v_s = 0$, $v_b = 1$ van der Waals levels were 0.988×10^{-3} and $0.722\times10^{-3}\ \text{cm}^{-1}$, respectively. The corresponding values obtained by Roncero *et al.* were 1.03×10^{-3} and $0.826\times10^{-3}\ \text{cm}^{-1}$.[35] Convergence of the results with respect to the initial and final values of R and the section width was checked. Given the differences in numerical methods and potential fitting, we feel that this level of agreement is sufficient to demonstrate the accuracy of our computer program.

All the vibrational predissociation results for Ar–OH described in this section have been obtained for total angular momentum $\mathscr{J} = 0.5$ and positive parity. The molecular parameters used for OH and OD are summarized in Table V.[75] The vibrationally averaged matrix elements over the interaction potential derived from the *ab initio* calculation described in Sec. VI is used in the remainder of this paper unless otherwise stated.

For vibrational predissociation of Ar–OH ($A\,^2\Sigma^+$, $v = 1$) the zeroth-order energies and wave functions of the quasibound states were obtained using the $V_{11}(R,\theta)$ potential. In order to judge the sensitivity of the van der Waals vibrational states to changes in the diatomic internuclear coordinate, we also computed the bound rovibrational eigenvalues and eigenfunctions of the $V_{00}(R,\theta)$ potential. The final state wave functions correspond to continuum levels associated with the $V_{00}(R,\theta)$ potential.

We used the adiabatic angular-radial separation technique, followed by bend-stretch optimization, to generate the radial basis. The adiabatic angular Hamiltonian corresponding to both the $v = 0$ and $v = 1$ was diagonalized at 330 unequally spaced values of R to give the effective potential of lowest energy. The bound radial eigenvalues were found to be converged to at least $0.01\ \text{cm}^{-1}$ with a basis of 167 equally spaced Gaussian functions distributed over a range of 4.0–24.0 bohr and 16 Gauss–Hermite quadrature points. We found that six iterative cycles to optimize for bend–stretch coupling were sufficient to converge the 40 eigenvalues of lowest energy of the radial and angular basis to $0.001\ \text{cm}^{-1}$.

Since the $V_{00}(R,\theta)$ and $V_{11}(R,\theta)$ potentials had surprisingly different well depths and anisotropies, it was necessary to use different basis sets to obtain comparable convergence for the two sets of van der Waals rovibrational levels. In the case of the $V_{00}(R,\theta)$ potential, setting the maximum value of the diatomic rotational angular momentum, $J_{\rm max}$, to 25.5 was adequate to converge the first 30 angular eigenvalues in order of increasing energy for $\mathscr{J} = 0.5$ to approximately $0.001\ \text{cm}^{-1}$. In the case of the $V_{11}(R,\theta)$ potential a value of $J_{\rm max} = 35.5$ was necessary to converge the first 30 eigenvalues to about $0.001\ \text{cm}^{-1}$ when $\mathscr{J} = 0.5$. When calculating the final rovibrational energies and wave functions for $V_{00}(R,\theta)$ with $\mathscr{J} = 0.5$ a basis set size of $N_{\rm str} = 30$, $N_{\rm ang} = 20$, and $N_x = 30$ was sufficient to converge the ten bound eigenvalues of lowest energy to better than $0.01\ \text{cm}^{-1}$. In the case of the $V_{11}(R,\theta)$ potential a basis set of size $N_{\rm str} = 40$, $N_{\rm ang} = 30$, and $N_x = 50$ was used. The rovibrational levels of the complex supported by the $V_{00}(R,\theta)$ and $V_{11}(R,\theta)$ potentials are listed in Tables VI and VII, respectively. Note that the corresponding energy levels in Tables VI and VII are not very similar and the energy levels for $V_{00}(R,\theta)$ are quite different than those obtained with r fixed in its equilibrium position.[27] These differences are due to the strong dependence of the intermolecular potential on the OH vibrational coordinate r.

When using the DVGR approximation, it is economical in terms of computer time to use a relatively small bound state basis since the evaluation of the driving term, defined in Eq. (30), must be carried out several hundred times in order to determine a single linewidth. The zeroth-order wave functions for the quasibound states supported by the vibrationally averaged interaction potential, $V_{11}(R,\theta)$, for Ar–OH ($A\,^2\Sigma^+$) were calculated using a small bound state basis of size $N_{\rm str} = 10$, $N_{\rm ang} = 10$, and $N_x = 20$. A comparison of the binding energies of the van der Waals levels given in Tables VI and VII indicates that levels $n = 1$–6 are converged to 0.1

TABLE V. Data for OH ($A\,^2\Sigma^+$) and OD ($A\,^2\Sigma^+$).[75]

	Vibrational state	Vibrational energy (cm^{-1})	Rotor constant (cm^{-1})	Spin–rotation constant (cm^{-1})
OH ($A\,^2\Sigma^+$)	$v=0$	1566.2	16.9646	0.201
	$v=1$	4559.2	16.1778	0.196
OD ($A\,^2\Sigma^+$)	$v=0$	1145.5	9.0346	0.120
	$v=1$	3360.8	8.7164	0.117

TABLE VI. Energies and assignments for some rovibrational bound states with $\mathscr{T} = 0.5, p = 1$ for the excited electronic state [asymptotic: Ar–OH($A\ ^2\Sigma^+, v' = 0$)] calculated with a basis set of size $N_{str} = 30$, $N_{ang} = 20$, and $N_x = 30$. The Ar–OH ($A\ ^2\Sigma^+$) interaction potential averaged over the OH $v = 0$ vibrational state was used to calculate the van der Waals (vdw) rovibrational levels.

		Stretch		Bend			
n[a]	Binding energy, (cm^{-1})	v_s	Component[b]	v_b	Component[b]	Rotor constant[c] (cm^{-1})	$\cos^{-1}\langle\cos\theta\rangle$[d] (degree)
1	−621.01	0	0.99	0	0.99	0.167	16.8
2	−483.77	1	0.99	0	0.99	0.160	17.7
3	−364.27	2	0.97	0	0.97	0.152	19.0
4	−262.68	3	0.93	0	0.94	0.142	20.9
5	−229.98	0	0.87	1	0.98	0.159	25.8
6	−179.34	4	0.83	0	0.88	0.131	23.8
7	−133.67	1	0.52	1	0.93	0.147	29.0
		2	0.30				
8	−114.58	5	0.64	0	0.78	0.119	29.0
		6	0.24	3	0.16		
9	−67.67	5	0.18	0	0.62	0.105	40.4
		6	0.34	3	0.21		
		7	0.41	8	0.14		
10	−63.09	1	0.20	1	0.76	0.130	37.4
		2	0.11	6	0.19		
		3	0.37				
		4	0.22				
11	−49.87	0	0.13	2	0.71	0.122	136.3
		1	0.11	5	0.21		
		2	0.20				
		3	0.19				
		4	0.19				
		5	0.10				
12	−36.12	6	0.22	0	0.39	0.093	66.9
		7	0.11	2	0.10		
		8	0.43	3	0.16		
		9	0.13	8	0.20		
13	−31.20	0	0.32	2	0.60	0.121	120.7
		5	0.18	5	0.15		
		6	0.13				
14	−25.43	5	0.28	1	0.38	0.106	62.1
		6	0.29	6	0.25		
		7	0.13	7	0.10		
				10	0.20		

[a] Label for rovibrational states.

[b] Fractional contribution of radial stretching basis function ψ^k_{str} with v_s quanta in the vdW stretching mode is $\Sigma_i |d^{n\mathscr{T}p^{2S+1}\Lambda}_{(i,k)}|^2$, where i denotes an angular basis function. Fractional contribution of a bending wave function is similarly defined.

[c] Calculated rotor constant $= \sum_{m=1}^{N_{max}} \sum_{m'=1}^{N_{max}} d^{n\mathscr{T}p^{2S+1}\Lambda}_{m} d^{n\mathscr{T}p^{2S+1}\Lambda}_{m'} \langle \psi^k_{str} | 1/2\mu R^2 | \psi^{k'}_{str} \rangle$.

[d] $\langle\cos\theta\rangle = \sum_{m=1}^{N_{max}} \sum_{m'=1}^{N_{max}} d^{n\mathscr{T}p^{2S+1}\Lambda}_{m} d^{n\mathscr{T}p^{2S+1}\Lambda}_{m'} \langle \psi^{J,\mathscr{T},\mathscr{M}p^{2S+1}\Lambda}_{ang} | \cos\theta | \psi^{J,\mathscr{T},\mathscr{M}p^{2S+1}\Lambda}_{ang} \rangle$.

cm^{-1} with the basis. The convergence for $n = 7$–10 is poorer; however, the small basis still yields energies within 2 cm^{-1} of the converged value for $n = 10$. This small basis, therefore, provides a reasonably accurate representation for the low energy bound states.

The linewidths and the final state distributions due to vibrational predissociation are obtained using the $\mathscr{R}$-matrix method described in Sec. IV. It is necessary to converge the $\mathscr{R}$-matrix results with respect to four parameters: (i) the constant sector width or step size h, (ii) the number of rotational channels N_{ch} associated with the final manifold, (iii) the initial value of R, R_O, at which propagation of the continuum wave functions is initiated, and (iv) the final value of R, R_A, at which the asymptotic boundary conditions are applied. The convergence tests[58] show that the linewidths are converged to within 0.1% for the parameter values of $N_{ch} = 41$, $h = 0.02$ bohr, $R_O = 3.5$ bohr, and $R_A = 25.0$ bohr. This set of parameters was used for all the scattering calculations on Ar–OH ($A\ ^2\Sigma^+$) reported in this paper.

C. Calculated linewidths, vibrational shifts, and product rotational distributions

The energies, assignments, and some structural parameters for the bound states of lowest energy supported by the $V_{00}(R,\theta)$ and $V_{11}(R,\theta)$ potentials is given in Tables VI and VII. Stretching, v_s, and bending, v_b, quantum numbers can be assigned by examining coefficients of product basis func-

TABLE VII. Energies and assignments for some rovibrational bound states with $\mathscr{T} = 0.5, p = 1$ for the excited electronic state [asymptotic Ar–OH ($A\ ^2\Sigma^+, v = 1$)] calculated with a basis set of size $N_{str} = 40$, $N_{ang} = 30$, and $N_x = 50$. The Ar–OH ($A\ ^2\Sigma^+$) interaction potential averaged over the OH $v = 1$ vibrational state was used to calculate the van der Waals rovibrational levels. (Notes as in Table III.)

		Stretch		Bend			
n[a]	Binding energy, (cm^{-1})	v_s	Component[b]	v_b	Component[b]	Rotor constant[c] (cm^{-1})	$\cos^{-1}\langle\cos\theta\rangle$[d] (degree)
1	−823.95	0	0.99	0	0.99	0.170	15.8
2	−664.98	1	0.99	0	0.99	0.164	16.6
3	−524.20	2	0.98	0	0.98	0.156	17.5
4	−401.32	3	0.96	0	0.96	0.148	18.7
5	−399.75	0	0.93	1	0.99	0.165	23.7
6	−296.31	4	0.91	0	0.92	0.139	20.4
7	−276.11	1	0.73	1	0.97	0.155	25.4
8	−209.57	5	0.80	0	0.87	0.129	23.0
9	−174.14	1	0.16	1	0.91	0.145	28.0
		2	0.43				
		3	0.33				
10	−141.39	5	0.12	0	0.77	0.117	27.3
		6	0.59	2	0.17		
		7	0.26				
11	−95.68	2	0.22	1	0.79	0.131	32.9
		4	0.39	5	0.18		
		5	0.21				
12	−89.66	6	0.19	0	0.65	0.106	33.7
		7	0.32	2	0.21		
		8	0.41	7	0.10		
13	−63.83	0	0.58	2	0.93	0.153	33.3
		1	0.30				
14	−50.25	7	0.21	0	0.52	0.095	44.3
		8	0.11	2	0.21		
		9	0.51	7	0.15		
15	−45.86	3	0.13	1	0.54	0.110	45.1
		5	0.14	5	0.28		
		6	0.33	10	0.16		
		7	0.23				
16	−39.13	2	0.15	3	0.75	0.118	140.5
		3	0.20	6	0.20		
		4	0.21				
		5	0.16				

tions $\psi^k_{str}\psi^{i\mathscr{T},\mathscr{E}p^{2S+1}\Lambda}_{ang}$. The rotor constants relate approximately to the intermolecular distance in a particular vibrational state. The $\cos^{-1}\langle\cos\theta\rangle$ quantity is useful for providing an idea of the degree of localization of a particular bending vibrational mode.

The D_0 value using the V_{00} potential is 621 cm^{-1} compared to the previously reported value of 597 cm^{-1} obtained when r was held fixed at 1.95 bohr.[27] The lower energy levels are well ordered, and it is possible to assign good v_s and v_b quantum numbers. Levels within a 100 cm^{-1} of the dissociation limit are, however, highly mixed bend–stretch combination bands that cannot be assigned in terms of separable vibrational modes. A noticeable feature of the rovibrational levels is the set of stretching vibrations, $v_s = 0$–5, associated with the ground bend (see levels with $n = 1$–4, 6, and 8 in Table VI). Levels with $n = 5$ and 7 involve the first excited bending state. The $\cos^{-1}\langle\cos\theta\rangle$ values indicate that the ground and first excited bend are localized in the Ar–H–O well. The second excited bend ($n = 12, 15$) is fairly high in energy and is localized in the Ar–O–H well.

The V_{11} potential is significantly different from the V_{00} potential and leads to a D_0 value of 824 cm^{-1}. The main stretching progression contains an additional $v_s = 6$ member. The $v_b = 0$, 1, and 2 bending vibrations are localized in the Ar–H–O well and only the $v_b = 3$ bend is localized in the Ar–O–H well, because for the V_{11} potential the minima at $\theta = 180°$ is much shallower than for the V_{00} potential. Experimental results indicate that the D_0 value should increase by approximately 30 cm^{-1} on exciting OH from the $v = 0$ to the $v = 1$ level.[31] This discrepancy between theory and experiment might be attributed to the neglect of off-diagonal vibrational matrix elements in our rovibrational calculations. The ideal way to eliminate this is to solve the rovibrational problem without separating the diatomic vibrational motion. Since this is computationally very expensive, we have performed a simple test to estimate the effect of neglecting the off-diagonal terms. This was done by considering a two-level problem involving the mixing of the $\phi_{v=0}(r)$ and

$\phi_{v=1}(r)$ wave functions due to the $V_{10}(R,\theta)$ term. For a given value of R and θ, the zeroth-order energies of the two states are given by $E_v + V_{vv}(R,\theta)$, where E_v is the vibrational energy of the isolated diatom. The perturbation of the zeroth-order wave functions by the V_{10} potential can be obtained to first order by diagonalizing the matrix,

$$\begin{pmatrix} E_v + V_{00}(R,\theta) & V_{10}(R,\theta) \\ V_{10}(R,\theta) & E_v + V_{11}(R,\theta) \end{pmatrix},$$

to provide two values of the intermolecular interaction energy: E_- correlating with the $v=0$ levels of OH and E_+ correlating with the $v=1$ levels of OH. The V_{00}, V_{11}, V_{10}, E_-, and E_+ values for a few geometries are listed in Table VIII. The effect of the V_{10} term can be seen to be about 80 cm^{-1} in the region of the van der Waals minimum. Inclusion of higher OH vibrational states might bring the differences between the D_0 values for the $v=0$ and $v=1$ states in closer agreement with experiment.

The calculated vibrational predissociation linewidths and lifetimes for the ten metastable van der Waals levels of lowest energy of Ar–OH ($A\,^2\Sigma^+$, $v=1$) are shown in Table IX. The associated final or product rotational distributions are shown in Table X. A comparison of the experimental linewidths given in Table IV with the calculated ones shows that the experimental linewidths are broader than the calculated linewidths by at least a factor of 30. The calculated and experimental shifts in the D_0 values also differ by a factor of about 7. While this level of disagreement between experiment and theory is disappointing at first sight, it is informative to explore the reasons for the discrepancy.

Inaccuracy of the theoretical calculation may stem from either inaccuracies in the *ab initio* potential or from limitations of the DVGR approximation. A similar Golden Rule calculation on the highly anisotropic $(HF)_2$ dimer resulted in a linewidth of 1.65×10^{-3} cm^{-1} for the ground van der Waals vibrational level.[37] This value was lower than the experimental result by approximately a factor of 4. Such calculated linewidths are of the same order of magnitude as our calculated linewidths for the highly anisotropic Ar–OH ($A\,^2\Sigma^+$) complex. It is, therefore, possible that in order to obtain broader linewidths it is necessary to go beyond the Golden Rule approximation and incorporate the effect of higher vibrational levels. The DVGR calculations on Ne–ICl, however, agree very well with the results of a full close-coupled photofragmentation calculation[35] and are of the same order of magnitude as the calculated linewidths for Ar–OH ($A\,^2\Sigma^+$). The *ab initio* potential appears to overestimate the difference between the $V_{11}(R,\theta)$ and $V_{00}(R,\theta)$ in terms of both anisotropy and well depth. The fact that the calculated linewidths are much smaller than the experimental linewidths may be partly due to the poor overlap of bound and scattering wave functions because of the relatively large difference in vibrationally averaged interaction potentials for the initial and final vibrational states. We have performed some approximate calculations to investigate the sensitivity of the predissociation linewidths to the potential anisotropy. While refinements in both theory and experiment are needed to obtain better numerical agreement between theory and experiment, we feel the present calculation

TABLE IX. Calculated linewidths (FWHM), lifetimes, and related data for the vibrational predissociation of the ten van der Waals levels of lowest energy of Ar–OH ($A\,^2\Sigma^+$, $v=1$) at $\mathscr{T}=0.5$, $p=1$. Explanation of column headings: n, label to designate van der Waals vibrational states in order of increasing energy; E_n, binding energy of van der Waals level "n" relative to the lowest rotational state of OH ($A\,^2\Sigma^+$, $v=1$); v_s, intermolecular stretching quantum number; v_b, bending quantum number; $E_v = 2993$ cm^{-1}, difference in vibrational energy of OH ($A\,^2\Sigma^+$, $v=1$) and OH ($A\,^2\Sigma^+$, $v=0$) (see Table V); $E_v + E_n$, energy of quasibound level relative to the ground rovibrational level of OH ($A\,^2\Sigma^+$); Γ_n; linewidth (FWHM) of level "n"; τ_n, lifetime of level "n"; N_{max}, maximum rotational angular momentum of diatom permitted energetically on vibrational predissociation; and E_{max}, maximum rotational energy of diatom permitted energetically on vibrational predissociation.

n	E_n (cm^{-1})	v_s	v_b	E_v+E_n (cm^{-1})	Γ_n (cm^{-1})	τ_n (ns)	N_{max}	E_{max} (cm^{-1})
1	−823.95	0	0	2169.1	0.004 79	1.11	10	1867.1
2	−664.98	1	0	2328.0	0.003 75	1.41	11	2240.4
3	−524.19	2	0	2468.8	0.002 73	1.94	11	2240.4
4	−401.30	3	0	2591.7	0.002 11	2.52	11	2240.4
5	−399.72	0	1	2593.3	0.006 07	0.87	11	2240.4
6	−296.26	4	0	2696.8	0.001 71	3.10	12	2647.7
7	−275.84	1	1	2717.2	0.005 87	0.90	12	2647.7
8	−209.18	5	0	2783.8	0.001 38	3.85	12	2647.7
9	−171.75	2	1	2821.3	0.004 64	1.14	12	2647.7
10	−139.34	6	0	2853.7	0.001 15	4.62	12	2647.7

TABLE VIII. Coupling of the OH ($A\,^2\Sigma^+$) vibrational wave functions by the interaction potential.

R (bohr)	θ (degrees)	$V_{00}(R,\theta)$[a] (cm^{-1})	$V_{11}(R,\theta)$[a] (cm^{-1})	$V_{10}(R,\theta)$[a] (cm^{-1})	E^b_- (cm^{-1})	E^c_+ (cm^{-1})
5.5	0.0	−1110.9	−1331.2	−337.2	−1151.3	−1290.8
	180.0	−280.1	−225.4	30.9	−280.4	−225.1
4.5	0.0	2785.9	3415.0	391.19	2744.1	3456.7
	180.0	−819.3	−678.5	290.4	−846.0	−651.8

[a] Vibrational matrix elements over the intermolecular interaction potential.
[b] Value of interaction energy at given R, θ for OH ($A\,^2\Sigma^+$, $v=0$) on including the effect of the $V_{10}(R,\theta)$ term by a first-order perturbation method.
[c] Value of interaction energy at given R, θ for OH ($A\,^2\Sigma^+$, $v=1$) on including the effect of the $V_{10}(R,\theta)$ term by a first-order perturbation method.

TABLE X. Calculated final rotational distributions for the vibrational predissociation of the ten van der Waals levels of lowest energy of Ar–OH ($A\,^2\Sigma^+, v=1$) at $\mathscr{T}=0.5, p=1$. The percentage probability of obtaining a particular rotational state due to vibrational predissociation of a given quasibound state is shown. Explanation for column headings: n, label designating van der Waals vibrational states in order of increasing energy; v_s, intermolecular stretching quantum number; v_b, bending quantum number; and N, rotational angular momentum quantum number of diatom.

	$n=1$	$n=2$	$n=3$	$n=4$	$n=5$	$n=6$	$n=7$	$n=8$	$n=9$	$n=10$
	$v_s=0$	$v_s=1$	$v_s=2$	$v_s=3$	$v_s=0$	$v_s=4$	$v_s=1$	$v_s=5$	$v_s=2$	$v_s=6$
N	$v_b=0$	$v_b=0$	$v_b=0$	$v_b=0$	$v_b=1$	$v_b=0$	$v_b=1$	$v_b=0$	$v_b=1$	$v_b=0$
0	0.21	0.55	1.17	2.06	0.00	3.36	0.00	4.65	0.00	5.14
1	0.02	0.04	0.08	0.10	0.02	0.18	0.06	0.32	0.12	0.44
2	0.41	1.12	2.34	4.15	0.00	5.53	0.01	6.91	0.02	7.21
3	0.06	0.19	0.41	0.77	0.03	1.35	0.10	1.99	0.20	2.33
4	0.57	1.60	2.91	3.96	0.02	4.55	0.05	5.25	0.09	5.57
5	0.11	0.43	0.97	1.65	0.12	2.63	0.33	3.69	0.68	4.22
6	0.60	1.50	2.12	2.07	0.07	1.85	0.16	1.83	0.29	1.66
7	0.27	1.25	2.51	2.72	0.38	2.63	0.96	3.14	1.83	3.64
8	3.28	6.94	9.60	10.13	0.50	10.29	1.14	10.99	1.98	10.18
9	18.33	26.16	27.77	24.50	0.22	21.53	0.38	20.24	0.55	18.51
10	76.13	43.18	30.04	25.65	2.05	18.73	3.19	13.92	4.36	13.10
11	⋯	17.00	20.05	22.23	96.57	26.19	85.16	25.94	79.83	27.14
12	⋯	⋯	⋯	⋯	⋯	1.17	8.46	1.12	10.03	0.83

is sufficiently accurate for analysis of trends in lifetimes and in final state distributions to be useful in providing insight into the vibrational predissociation process.

The vibrational predissociation linewidths for Ar–OH ($A\,^2\Sigma^+, v=1$) are plotted as a histogram in Fig. 1. It can be seen that the linewidths of quasibound levels with $v_b=0$ form a clear progression in which linewidth decreases with increase in the v_s quantum number. The associated final rotational distributions in Table X indicate that highly rotationally excited OH ($A\,^2\Sigma^+, v=0$) with $N>9$ will be the dominant product of vibrational predissociation. Thus Ar–OH ($A\,^2\Sigma^+, v=1$) predissociation is predominantly a vibration to rotation ($V\rightarrow R$), rather than a vibration to translation ($V\rightarrow T$), energy transfer process. The distribution for the $n=1$ level peaks strongly at $N=10$. With an increasing number of open channels available as the energy

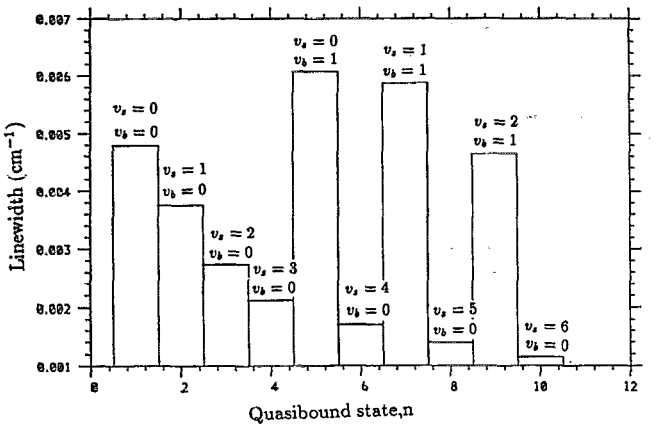

FIG. 1. Calculated vibrational predissociation linewidths (in cm^{-1}) of the ten van der Waals vibrational levels of lowest energy of Ar–OH ($A\,^2\Sigma^+$, $v=1$) at $\mathscr{T}=0.5, p=1$.

of the metastable levels with $v_b=0$ relative to the ground rovibrational state of OH ($A\,^2\Sigma^+$) increases, the final population distribution in levels with $N=9$–12 flattens out and for high v_s becomes bimodal. Such highly inverted product distributions can be produced by strong anisotropy in the coupling and final state potential. They can also be produced by the large changes in the $v=0$ and $v=1$ potentials used in the calculations. The details of the product state distribution are expected to be very sensitive to the final state interactions and a complete analysis is not possible given the likely inaccuracies in the potential. It is clear that a $V\rightarrow R, T$ transfer is most favorable for levels with $N=9$–12, but the anisotropy of the potential does not appear to be sufficient to excite $N=12$ levels appreciably. Given the basic similarity in the rotational distributions for the $v_b=0$ levels, one can qualitatively explain the trend of decreasing linewidth with increasing v_s using the momentum gap or energy gap law, which states the linewidth will decrease with increase in the final translational energy of the products.[76,77] We have not attempted any fit to the exponential form of the momentum gap law since this is clearly not a case of pure vibrational to translational energy transfer.

A comparison of the calculated linewidths of Ar–OH ($A\,^2\Sigma^+$) with those calculated for Ar–HCl ($X\,^1\Sigma^+$) in Ref. 45 are of interest. The vibrational frequencies of both Ar–OH ($A\,^2\Sigma^+$) and Ar–HCl are approximately 3000 cm^{-1}. The rotor constants of OH and HCl are about 17 and 10 cm^{-1}, respectively, and the calculated linewidths of Ar–OH ($A\,^2\Sigma^+$) and Ar–HCl ($X\,^1\Sigma^+$) are of the order of 10^{-3} and 10^{-6} cm^{-1}, respectively. Ar–HCl has a well depth of about 180 cm^{-1}. The larger well depth and anisotropy of Ar–OH in the first excited state clearly increases the calculated vibrational predissociation linewidths by several orders of magnitude even though our calculated linewidths are still an order of magnitude smaller when compared with experi-

ment. The product distribution for the ground van der Waals level of Ar–OH is very similar in shape to the distribution obtained for Ar–HCl vibrational predissociation.[45]

The quasibound levels with a common $v_b = 1$ assignment also show a distinct trend of decreasing linewidths with increasing energy (momentum gap law) but have significantly larger linewidths than levels with $v_b = 0$. The rotational distributions for the $v_b = 1$ levels have a very sharp maximum at $N = 11$ and do not change significantly with increasing v_s. The decompositions of the initial bound state function for the ($v_s = 0$, $v_b = 1$) and ($v_s = 3$, $v_b = 0$) levels in terms of the free rotor function of OH ($A\,^2\Sigma^+$) are shown in Fig. 2. The corresponding final state distributions are also shown on the same figure. The initial distribution for the $v_b = 1$ level has a minimum at $N = 0$, in contrast to the $v_b = 0$ distribution. The initial distribution for the first excited bend has a maximum at a higher value of N than the distribution for the ground bending level.

D. Effect of anisotropy

The anisotropy of the potential is shown in the calculations to be an important factor controlling vibrational to rotational energy transfer and linewidths. We mentioned the possible effects of relative anisotropy of the initial and final vibrational states on the linewidths in the previous section. In this section we consider the effect of changing the overall anisotropy of the interaction potential. To test the sensitivity of the total linewidths to the anisotropy, we multiplied the anisotropic terms in the Legendre expansions of the $V_{11}(R,\theta)$, $V_{10}(R,\theta)$ and $V_{00}(R,\theta)$ potentials by a constant factor. The energies and linewidths of the quasibound states were recalculated with a bound state basis of $N_{\rm str} = 10$, $N_{\rm ang} = 10$, $N_x = 20$, and $\mathscr{R}$-matrix parameters $h = 0.02$ bohr, $R_A = 25.0$ bohr, $R_O = 3.5$ bohr, and $N_{\rm ch} = 41$. The energies, vibrational assignments, and linewidths when the anisotropic terms were multiplied by factors of 1.1 (set A) and 0.9 (set B) are reported in Table XI. Comparison with the

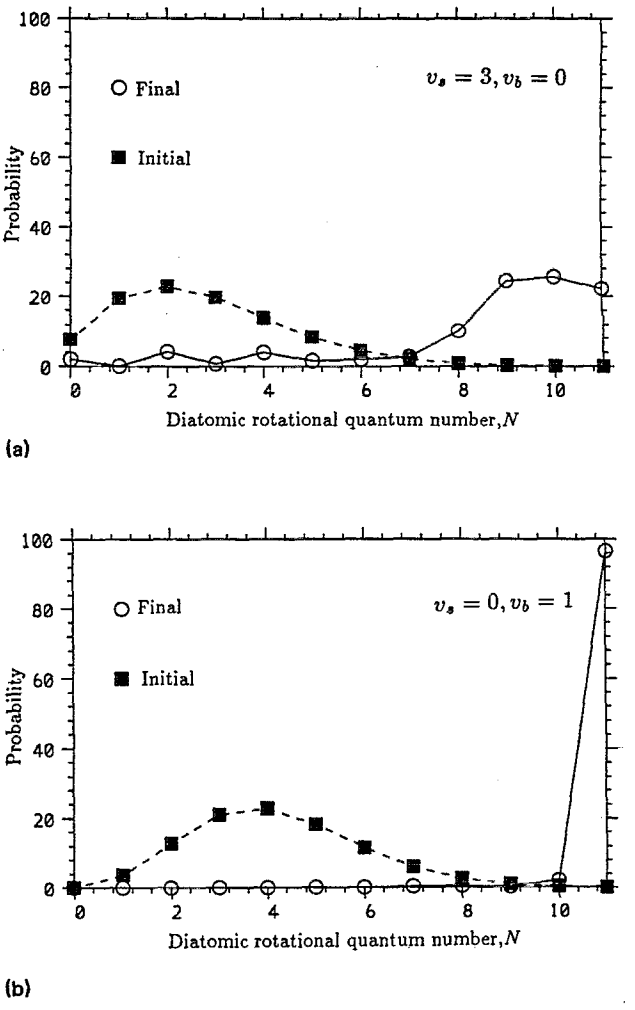

FIG. 2. Calculated initial and final rotational distributions of the van der Waals vibrational levels ($v_s = 3$, $v_b = 0$) and ($v_s = 0$, $v_b = 1$) of Ar–OH ($A\,^2\Sigma^+$, $v = 1$) at $\mathscr{T} = 0.5$, $p = 1$.

TABLE XI. Change in linewidths (Γ_n) with change in anisotropy. Explanation for column headings: [a] Calculations in sets A and B were carried out after multiplying the anisotropic terms in the Legendre expansion of the *ab initio* potential by factors of 1.1 and 0.9, respectively; n, label designating van der Waals vibrational states in order of increasing energy; v_s, intermolecular stretching quantum number; v_b, bending quantum number; and Γ_n: Linewidth (FWHM) for level "n."

n	A[a]				B[a]			
	E_n (cm^{-1})	v_s	v_b	Γ_n (cm^{-1})	E_n (cm^{-1})	v_s	v_b	Γ_n (cm^{-1})
1	−971.56	0	0	0.010 04	−683.58	0	0	0.001 90
2	−796.77	1	0	0.004 69	−540.83	1	0	0.001 14
3	−640.67	2	0	0.003 79	−415.80	2	0	0.001 02
4	−514.29	0	1	0.020 78	−308.57	3	0	0.000 81
5	−502.78	3	0	0.002 99	−295.40	0	1	0.003 05
6	−382.72	4	0	0.002 02	−219.54	4	0	0.000 64
7	−373.15	1	1	0.010 34	−189.34	1	1	0.000 73
8	−280.35	5	0	0.001 64	−148.83	5	0	0.000 50
9	−252.46	2	1	0.006 12	−102.71	2	1	0.000 63
10	−195.44	6	0	0.001 40	−93.86	6	0	0.000 37

linewidths in Table IX shows that increasing the anisotropy by about 10% increases the linewidths by factors of 1.5–3 and decreasing the anisotropy by 10% decreases linewidths by a similar amount. Judging from the linewidths of the calculations reported the previous sections, an error of this order of magnitude in the anisotropic term would not be unexpected. It is, therefore, worthwhile to consider methods for improving the *ab initio* potential by fitting it to experiment.[22]

E. Effect of isotopic substitution

The difference between calculated linewidths for Ar–OH ($A\,^2\Sigma^+$, $v=1$) and Ar–OD ($A\,^2\Sigma^+$, $v=1$) stem from three causes. First, the vibrational spacings and rotor constants of OD relative to OH are dramatically reduced by factors of approximately 2/3 and 1/2, respectively (see Table V). Second, the interaction potential must be refitted,[28,29] but this is expected to result in minor changes. Third, the vibrationally averaged matrix elements over the interaction potential must be calculated using an RKR potential for OD rather than for OH. This might cause some significant changes in relative anisotropy of the initial and final states since the OD vibrational wave functions will correspond to smaller expectation values of the diatomic internuclear coordinate than the OH vibrational wave functions. We have not attempted to refit the potential and recalculate the vibrational matrix elements but have carried out an approximate vibrational predissociation calculation for Ar–OD ($A\,^2\Sigma^+$, $v=1$) by substituting the molecular parameters of OD instead of OH. The bound state basis used was $N_{\rm str}=10$, $N_{\rm ang}=15$, $N_x=25$, and the $\mathscr{R}$-matrix parameters were $h=0.02$ bohr, $R_A=25.0$ bohr, $R_O=3.5$ bohr, and $N_{\rm ch}=61$. The linewidths and rotational distributions produced by this calculation are reported in Tables XII and XIII, respectively.

TABLE XII. Calculated linewidths (FWHM), lifetimes, and related data for the vibrational predissociation of ten van der Waals levels of lowest energy of Ar–OD ($A\,^2\Sigma^+$, $v=1$) at $\mathscr{T}=0.5$, $p=1$. The vibrationally averaged matrix elements over the interaction potential for Ar–OH($A\,^2\Sigma^+$) were used in this calculation. Explanation of column headings: n, label designating van der Waals vibrational states in order of increasing energy; E_n, binding energy of van der Waals level "n" relative to the lowest rotational state of OD ($A\,^2\Sigma^+$, $v=1$); v_s, intermolecular stretching quantum number; v_b bending quantum number; $E_v=2215.3\ \text{cm}^{-1}$, difference in vibrational energy of OD ($A\,^2\Sigma^+$, $v=1$) and OD ($A\,^2\Sigma^+$, $v=0$) (see Table V); E_v+E_n, energy of quasibound state relative to ground rovibrational level of OD ($A\,^2\Sigma^+$); Γ_n, linewidth (FWHM) of level "n," τ_n, lifetime of level "n;" $N_{\rm max}$, maximum rotational angular momentum of diatom permitted energetically on vibrational predissociation; and $E_{\rm max}$, maximum rotational energy of diatom permitted energetically on vibrational predissociation.

n	E_n (cm^{-1})	v_s	v_b	E_v+E_n (cm^{-1})	Γ_n (cm^{-1})	τ_n (ns)	$N_{\rm max}$	$E_{\rm max}$ (cm^{-1})
1	−935.79	0	0	1279.5	0.003 61	1.47	11	1193.2
2	−769.01	1	0	1446.3	0.002 95	1.80	12	1410.1
3	−619.90	2	0	1595.4	0.002 13	2.49	12	1410.1
4	−610.12	0	1	1605.2	0.006 82	0.78	12	1410.1
5	−488.12	3	0	1727.2	0.001 65	3.22	13	1645.1
6	−466.91	1	1	1748.4	0.005 15	1.03	13	1645.1
7	−373.44	4	0	1841.8	0.001 61	3.30	13	1645.1
8	−343.23	2	1	1872.1	0.004 35	1.22	13	1645.1
9	−324.98	0	2	1890.3	0.011 79	0.45	13	1645.1
10	−275.89	5	0	1939.4	0.001 72	3.09	14	1898.1

It can be seen from Table XII that the linewidths for Ar–OD ($A\,^2\Sigma^+$, $v=1$) compared to those for Ar–OH ($A\,^2\Sigma^+$), $v=1$) are smaller by a factor of 1.5 for the $v_b=0$ quasibound levels. The linewidths for the $v_b=1$ levels are similar for both complexes. The $v_b=2$ level, reported only

TABLE XIII. Calculated final rotational distributions for the vibrational predissociation of the ten van der Waals levels of lowest energy of Ar–OD ($A\,^2\Sigma^+$, $v=1$) at $\mathscr{T}=0.5$, $p=1$. The vibrationally averaged matrix elements over the interaction potential for Ar–OH ($A\,^2\Sigma^+$) were used in this calculation. The percentage probability of obtaining a particular rotational state due to vibrational predissociation of a given quasibound state is shown. Explanation for column headings: n, label designating van der Waals vibrational states in order of increasing energy; v_s, intermolecular stretching quantum number; v_b, bending quantum number; and N, rotational angular momentum quantum number of diatom.

	$n=1$	$n=2$	$n=3$	$n=4$	$n=5$	$n=6$	$n=7$	$n=8$	$n=9$	$n=10$
	$v_s=0$	$v_s=1$	$v_s=2$	$v_s=0$	$v_s=3$	$v_s=1$	$v_s=4$	$v_s=2$	$v_s=0$	$v_s=5$
N	$v_b=0$	$v_b=0$	$v_b=0$	$v_b=1$	$v_b=0$	$v_b=1$	$v_b=0$	$v_b=1$	$v_b=2$	$v_b=0$
0	1.64	3.29	5.41	0.01	7.59	0.00	9.93	0.00	0.77	11.00
1	0.59	1.54	3.09	0.91	6.46	2.49	10.04	4.04	0.12	12.21
2	2.44	2.46	1.47	0.16	0.44	0.89	0.81	2.04	0.91	1.73
3	5.01	9.57	10.17	0.95	8.23	1.64	6.73	2.34	0.63	6.31
4	7.70	10.01	8.97	0.15	5.64	0.84	3.28	1.42	0.58	2.41
5	9.78	11.70	8.54	2.17	5.36	4.79	3.63	5.89	0.95	3.34
6	22.64	26.67	23.98	0.42	21.50	0.49	20.22	0.32	0.16	19.36
7	18.49	21.84	22.32	10.30	19.99	20.55	20.50	23.80	0.56	20.08
8	1.68	1.51	7.00	14.01	11.07	25.07	13.43	26.24	0.60	14.02
9	14.70	2.99	1.67	6.39	2.46	3.80	3.11	1.20	2.26	3.26
10	12.66	1.40	1.64	21.48	3.24	19.08	2.61	13.19	3.29	2.16
11	2.66	3.72	4.86	26.75	6.94	14.00	5.29	6.58	15.08	3.35
12	⋯	3.25	0.86	16.30	0.10	0.92	0.12	2.35	32.34	0.24
13	⋯	⋯	⋯	⋯	0.97	5.42	0.29	10.58	41.74	0.49
14	⋯	⋯	⋯	⋯	⋯	⋯	⋯	⋯	⋯	0.01

for the OD complex, has a linewidth greater than any of the linewidths calculated for the OH complex. On deuterium substitution the vibrational spacing decreases and the vibrational coupling terms remain the same; this is expected to enhance the linewidths. However, the rotor constant of OD is half that of OH and consequently vibrational to rotational energy transfer is less favorable. This is expected to lead to a decrease in the linewidths. The changes in linewidths reported above must be explained in terms of an interplay between these two factors. We would like to point out that some inaccuracies will be generated from using the same vibrationally averaged potentials for Ar–OD ($A\,^2\Sigma^+$) and Ar–OH ($A\,^2\Sigma^+$) and an accurate potential would be expected to lead to a result in closer accord with experiment. The calculated rotational distributions are reported in Table XIII. As expected from the change in linewidth, the final rotational distributions for levels with $v_b = 0$ are far less rotationally excited (peak at $N = 6, 7$) for the OD complex than for the OH complex. The $v_b = 1$ levels have final state distributions with maxima in the region of $N = 10$. The $v_b = 2$ level dissociates to form OD ($A\,^2\Sigma^+, v = 0$) in mostly $N = 11$ and 12 levels. For a given value of v_b the trends in linewidths with v_s are qualitatively explained by the momentum gap law.[76,77]

VI. CONCLUSIONS

An $\mathscr{R}$-matrix algorithm is developed for executing vibrational predissociation calculations within the Golden Rule approximation. Vibrational predissociation linewidths and product rotational distributions for the quasibound states of Ar–OH ($A\,^2\Sigma^+, v = 1$) are calculated using this technique. The dependence of the *ab initio* intermolecular potential on the diatomic internuclear distance is calculated using the CEPA method. These computed vibrational predissociation linewidths, although being surprisingly broad ($> 10^{-3}$ cm^{-1}) for a weakly bonded complex containing a diatomic monomer with a large vibrational frequency, are smaller than the experimental results by over an order of magnitude. This suggests that improvements are needed in the potential energy surface, which is found to be surprisingly sensitive to the OH vibrational coordinate.

Approximate calculations are presented to show that relatively small changes in potential anisotropy, of the order of ten percent, can lead to significant changes in the predissociation linewidths. Certain qualitative trends in linewidths and product rotational distributions are established. The high anisotropy of the system is found to strongly favor vibrational to rotational energy transfer; consequently, most of the OH ($A\,^2\Sigma^+, v = 0$) produced is expected to be in highly excited rotational states. Quasibound states associated with excited bending levels are predicted to dissociate more rapidly than those assigned to the ground bend. For metastable states with the same bending quantum number, calculated linewidths decrease with increase in the intermolecular stretching quantum number. A calculation on vibrational predissociation in Ar–OD ($A\,^2\Sigma^+$) is carried out without refitting the potential to account for isotopic substitution. This calculation indicates that most linewidths for quasibound states of Ar–OD ($A\,^2\Sigma^+, v = 1$) are expected to be smaller than for Ar–OH ($A\,^2\Sigma^+, v = 1$). Vibrational to rotational energy transfer for the OD complex is less favorable than for the OH complex.

ACKNOWLEDGMENTS

This research was supported by the Science and Engineering Research Council (SERC), the Deutsche Forschungsgemeinschaft, and the Fonds der Chemischen Industrie. C.C. is grateful to Churchill College for a research studentship. ADE would like to thank the Italien CNR for a grant. The authors would like to thank M. I. Lester, M. T. Berry, and W. M. Fawzy for useful discussion and M. H. Alexander for the use of his *Hibridon* program.

[1] J. A. Beswick and J. Jortner, Adv. Chem. Phys. **47**, 363 (1981).
[2] D. J. Nesbitt, Chem. Rev. **88**, 843 (1988).
[3] D. H. Levy, Adv. Chem. Phys. **47**, 323 (1981).
[4] *Structure and Dynamics of Weakly Bound Molecular Complexes*, edited by A. Weber (Reidel, Dordrecht, 1987).
[5] Faraday Discuss. Chem. Soc. **73**, (182).
[6] K. C. Janda, Adv. Chem. Phys. **60**, 201 (1985).
[7] K. C. Janda and F. G. Celii, Chem. Rev., **86**, 507 (1986).
[8] D. C. Clary, J. Phys. Chem. **91**, 1718 (1987).
[9] *Dynamics of Polyatomic van der Waals Complexes*, edited by N. Halberstadt and K. C. Janda (Plenum, New York, 1990).
[10] P. D. A. Mills, C. M. Western, and B. J. Howard, J. Phys. Chem. **90**, 3331 (1986); P. D. A. Mills, C. M. Western, and B. J. Howard, J. Phys. Chem. **90**, 4961 (1986).
[11] G. C. Nielson, G. A. Parker, and R. T Pack, J. Chem. Phys. **66**, 1396 (1977).
[12] S. Miller, J. Tennyson, B. Follmeg, P. Rosmus, and H.-J. Werner, J. Chem. Phys. **89**, 2178 (1988).
[13] A. van der Avoird, J. Chem. Phys. **79**, 1170 (1983).
[14] A. van der Avoird and G. Brocks, J. Chem. Phys. **87**, 5346 (1987).
[15] J. Goodman and L. E. Brus, J. Chem. Phys. **67**, 4858 (1977).
[16] M. T. Berry, M. R. Brustein, and M. I. Lester, Chem. Phys. Lett. **153**, 17 (1988).
[17] M. T. Berry, M. R. Brustein, J. R. Adamo, and M. I. Lester, J. Phys. Chem. **92**, 5551 (1988).
[18] M. I. Lester, in *Dynamics of Polyatomic van der Waals Complexes*, edited by N. Halberstadt and K. C. Janda (Plenum, New York, 1990), p. 143.
[19] K. M. Beck, M. T. Berry, M. R. Brustein, and M. I. Lester, Chem. Phys. Lett. **162**, 203 (1989).
[20] W. M. Fawzy and M. C. Heaven, J. Chem. Phys. **89**, 7030 (1988); **92**, 909 (1990).
[21] W. M. Fawzy and J. T. Hougen, J. Mol. Spectrosc. **137**, 154 (1989).
[22] J. M. Bowman, B. Gazdy, P. Schafer, and M. C. Heaven, J. Phys. Chem. **94**, 2226 (1990).
[23] S. K. Bramble and P. A. Hamilton, Chem. Phys. Lett. **170**, 107 (1990).
[24] M. I. Lester, M. T. Berry, M. R. Brustein, C. Chakravarty, and D. C. Clary, Chem. Phys. Lett. **178**, 301 (1991).
[25] W. Meyer, Int. J. Quantum Chem. Symp. **5**, 341 (1971); W. Meyer, J. Chem. Phys. **58**, 1017 (1973).
[26] A. Degli Esposti and H.-J. Werner, J. Chem. Phys. **93**, 3351 (1990); the calculations were done using the MOLPRO package of *ab initio* computer programs written by H. -J. Werner and P. J. Knowles with contributions from J. Almlof, R. Amos, S. Elbert, W. Meyer, E. A. Reinsch, R. Pitzer, and A. J. Stone.
[27] C. Chakravarty, D. C. Clary, A. D. Esposti, and H.-J. Werner, J. Chem. Phys. **93**, 3367 (1990).
[28] C. Chakravarty and D. C. Clary, Chem. Phys. Lett. **173**, 541 (1990).
[29] C. Chakravarty and D. C. Clary, J. Chem. Phys. **94**, 4149 (1991).
[30] M. T. Berry, M. R. Brustein, and M. I. Lester, J. Chem. Phys. **90**, 5878 (1989).
[31] M. T. Berry, M. R. Brustein, and M. I. Lester, J. Chem. Phys. **92**, 6469 (1990).

[32]M. Shapiro and R. Bershon, Annu. Rev. Phys. Chem. **33**, 409 (1982).
[33]C. J. Ashton, M. S. Child, and J. M. Hutson, J. Chem. Phys. **78**, 4025 (1983).
[34]N. Halberstadt, J. A. Beswick, and K. C. Janda, J. Chem. Phys. **87**, 3966 (1987).
[35]O. Roncero, J. A. Beswick, N. Halberstadt, P. Villarreal, and G. Delgado-Barrio, J. Chem. Phys. **92**, 3348 (1990).
[36]R. L. Waterland, M. I. Lester, and N. Halberstadt, J. Chem. Phys. **92**, 4261 (1990).
[37]N. Halberstadt, Ph. Bréchignac, J. A. Beswick, and M. Shapiro, J. Chem. Phys. **84**, 170 (1986).
[38]R. T Pack. J. Chem. Phys. **60**, 633 (1974).
[39]R. J. Le Roy and J. S. Carley, Adv. Chem. Phys. **42**, 353 (1980).
[40]H. Lefebvre-Brion and R. W. Field, *Perturbation in the Spectra of Diatomic Molecules* (Academic, Orlando, FL, 1986).
[41]D. E. Manolopoulos, Ph.D thesis, University of Cambridge, 1988.
[42]J. N. Murrell and S. D. Bosanac, *Introduction to the Theory of Atomic and Molecular Collisions* (Wiley, Chichester, 1989).
[43]R. J. Le Roy, G. C. Corey, and J. M. Hutson, Faraday Discuss. Chem. Soc. **82**, 241 (1986).
[44]J. M. Hutson, C. J. Ashton, and R. J. Le Roy, J. Phys. Chem. **87**, 2713 (1983).
[45]J. M. Hutson, J. Chem. Phys. **81**, 2357 (1984).
[46]A. C. Peet, Ph.D thesis, University of Cambridge, 1987.
[47]M. D. Morse, K. F. Freed, and Y. B. Band, J. Chem. Phys. **70**, 3604 (1979).
[48]Y. B. Band, K. F. Freed, and D. J. Kouri, J. Chem. Phys. **74**, 4380 (1981).
[49]D. C. Clary, C. Chakravarty, and A. R. Tiller in *Dynamics of Polyatomic van der Waals Complexes*, edited by N. Halberstadt and K. C. Janda (Plenum, New York, 1990), p. 355.
[50]I. P. Hamilton and J. C. Light, J. Chem. Phys. **84**, 306 (1986).
[51]D. C. Clary and D. J. Nesbitt, J. Chem. Phys. **90**, 7000 (1989).
[52]M. H. Alexander, J. Chem. Phys. **76**, 3637 (1982).
[53]M. H. Alexander, J. Chem. Phys. **76**, 5974 (1982).
[54]M. H. Alexander and G. C. Corey, J. Chem. Phys. **84**, 100 (1986).
[55]H.-J. Werner, B. Follmeg, and M. H. Alexander, J. Chem. Phys. **89**, 3139 (1988).
[56]J. M. Brown, J. T. Hougen, K.-P. Huber, J. W. C. Johns, I. Kopp, H. Lefebvre-Brion, A. R. Merer, D. A. Ramsay, J. Rostas, and R. N. Zare, J. Mol. Spectrosc. **55**, 500 (1975).
[57]R. W. Heather and J. C. Light, J. Chem. Phys. **78**, 5513 (1983).
[58]C. Chakravarty, Ph.D. thesis, University of Cambridge, 1990.
[59]M. S. Child, *Molecular Collision Theory* (Academic, London, 1974).
[60]J. C. Light, in *The Theory of Chemical Reaction Dynamics*, edited by D. C. Clary (Reidel, Dordrecht, 1986), p. 215.
[61]J. C. Light and R. B. Walker, J. Chem. Phys. **65**, 4272 (1976).
[62](a) G. A. Parker, T. G. Schmalz, and J. C. Light, J. Chem. Phys. **73**, 1757 (1980); (b) E. B. Stechel, R. B. Walker, and J. C. Light, *ibid.* **69**, 3518 (1978).
[63]A. N. Brooks, Ph.D thesis, University of Cambridge, 1989.
[64]J. P. Henshaw, Ph.D thesis, University of Cambridge, 1986.
[65]K. C. Kulander and J. C. Light, J. Chem. Phys. **73**, 4337 (1980).
[66]R. W. Heather and J. C. Light, J. Chem. Phys. **79**, 147 (1983).
[67]D. C. Clary, J. Chem. Phys. **84**, 4288 (1986).
[68]R. B. Walker and E. F. Hayes, in *The Theory of Chemical Reaction Dynamics*, edited by D. C. Clary (Reidel, Dordrecht, 1986), p. 105.
[69]J. M. Skene, J. C. Drobits, and M. I. Lester, J. Chem. Phys. **85**, 2329 (1986).
[70]W. Lester, Methods Comput. Phys. **10**, 211 (1971).
[71]J. W. Cooley, Math. Comput. **15**, 363 (1961).
[72]R. J. Fallon, I. Tobias, and J. T. Vanderslice, J. Chem. Phys. **34**, 167 (1961).
[73]W. M. Fawzy and M. C. Heaven (private communication).
[74]S. Kulkarni, Y. Lin, and M. C. Heaven, Chem. Phys. Lett. **167**, 597 (1990).
[75]K. P. Huber and G. Herzberg, *Constants of Diatomic Molecules* (Van Nostrand, New York, 1979).
[76]G. E. Ewing, J. Chem. Phys. **72**, 2096 (1980).
[77]G. E. Ewing, J. Phys. Chem. **91**, 4662 (1987).